Mon. Not. R. Astron. Soc. **000**, 1–?? () Printed 8 February 2016 (MN LATEX style file v2.2)

Phase space dynamics of triaxial collapse: Joint density-velocity evolution

Sharvari Nadkarni-Ghosh[1⋆] and Akshat Singhal[2]†
[1] *Department of Physics, I.I.T. Kanpur, Kanpur, U.P. 208016 India*
[2] *Department of Mathematics and Statistics, I.I.T. Kanpur, Kanpur, U.P. 208016 India*

arXiv:1407.1945v4 [astro-ph.CO] 5 Feb 2016

ABSTRACT

We investigate the dynamics of triaxial collapse in terms of eigenvalues of the deformation tensor, the velocity derivative tensor and the gravity Hessian. Using the Bond-Myers model of ellipsoidal collapse, we derive a new set of equations for the nine eigenvalues and examine their dynamics in phase space. The main advantage of this form is that it eliminates the complicated elliptic integrals that appear in the axes evolution equations and is more natural way to understand the interplay between the perturbations.

This paper focuses on the density-velocity dynamics. The Zeldovich approximation implies that the three tensors are proportional; the proportionality constant is set by demanding 'no decaying modes'. We extend this condition into the non-linear regime and find that the eigenvalues of the gravity Hessian and the velocity derivative tensor are related as $\tilde{q}_d + \tilde{q}_v = 1$, where the triaxiality parameter $\tilde{q} = (\lambda_{\rm max} - \lambda_{\rm inter})/(\lambda_{\rm max} - \lambda_{\rm min})$. This is a *new universal relation* holding true over all redshifts and a range of mass scales to within a few percent accuracy. The mean density-velocity divergence relation at late times is close to linear, indicating that the dynamics is dictated by collapse along the largest eigendirection. This relation has a scatter, which we show, is intimately connected to the velocity shear. Finally, as an application, we compute the PDFs of the two variables and compare with other forms in the literature.

Key words: cosmology: large-scale structure of Universe

1 INTRODUCTION

Over the last decade or so, observations of the large scale structure in the universe have emerged as a very powerful probe to constrain cosmological parameters. The two main variables that characterize this structure are the fractional overdensity δ and the peculiar velocity $\mathbf{v}$. In the linear regime, the two observables are connected as $\nabla \cdot \mathbf{v} = -fH\delta$, where H is the Hubble parameter and f is the growth rate. f is sensitive to the underlying cosmology and surveys such as 6dFGS [1] or the future EUCLID [2] observe peculiar velocities either directly (e.g., Johnson et al. 2014) or from redshift space distortions (e.g.,Majerotto et al. 2012) with an aim to place precise constraints on f. It would be ideal if the data followed linear theory, but observations are sensitive to non-linear effects which can introduce a bias even on linear scales. Therefore, a theoretical understanding of the non-linear regime is imperative. Numerical simulations and perturbation theories are the two standard ways of tracking non-linear growth. However, both these methods have drawbacks. N-body codes are slow. Furthermore, they use a discrete representation of the density field and hence their results are shot-noise limited (for e.g., Joyce, Marcos, & Baertschiger 2009). Perturbation theories deal with smooth fields but they are not always guaranteed to converge and involved resummation techniques need to be invoked to get meaningful results (for e.g., Matsubara 2008; Matarrese & Pietroni 2007; Nadkarni-Ghosh & Chernoff 2011, 2013). Given the plethora of cosmological models, these features can prove to be restrictive.

⋆ E-mail: sharvari@iitk.ac.in
† E-mail: akshat.singhal014@gmail.com
[1] http://www.6dfgs.net/
[2] http://www.euclid-ec.org/

© RAS

A third way to model the non-linear regime is to restrict the dynamics to simple geometries. Though based on local dynamics, such models often give theoretical insight into the underlying physics. The simplest among these is the spherical collapse model (spherical top-hat). It has been used in a myriad of ways starting from the mid-seventies to the present day. The critical density for collapse predicted by this model is an important ingredient in the mass function prescription given by Press & Schechter (1974). It has been widely used to understand the nature of non-linearities in a range of dark energy cosmologies from ΛCDM to early dark energy and quintessence models (for e.g., see Wintergerst & Pettorino 2010 and references therein). Kitaura & Heß (2013) have used it in conjunction with Lagrangian perturbation theory to evolve perturbations through the shell-crossing regime. It has given valuable insights into the joint non-linear density-velocity evolution (Bilicki & Chodorowski 2008; Nadkarni-Ghosh 2013). It has also been proposed as a control case to test the accuracy of N-body codes in the non-linear regime (Joyce & Sylos Labini 2012). And last but not the least, it has been used to explain the famous NFW profile (Navarro, Frenk, & White 1996; Łokas 2000) and as well as results of other simulations based on modified gravity (Stabenau & Jain 2006; Martino, Stabenau, & Sheth 2009).

Ellipsoidal or triaxial collapse is the next popular local model. It provides many improvements over the spherical geometry and has been in consideration for over five decades. Early studies (Lynden-Bell 1964; Lin, Mestel, & Shu 1965) examined the isolated ellipsoid in a non-expanding background. Cosmological extensions were performed by Icke (1973) and White & Silk (1979) but under the assumption that the background did not exert external forces on the ellipsoid. Bond & Myers (1996) included the effect of the background in terms of an external tidal field. Nariai & Fujimoto (1972) and Eisenstein & Loeb (1995) provided a more complete analytic model that includes rotation as well. Since then, not much has changed in the theoretical ingredients of the model, however, the number of applications have been on the rise. Effects of non-radial motions on the growth rate and the resultant modifications to the Press-Schecter mass function were studied by several authors (for e.g., Monaco 1995; Del Popolo & Gambera 2000; Del Popolo, Ercan, & Xia 2001; Sheth, Mo, & Tormen 2001; Kerscher, Buchert, & Futamase 2001). Many authors developed alternatives to Press-Schecter that were based on statistics of collapse times derived from ellipsoidal collapse (Audit, Teyssier, & Alimi 1997; Monaco, Theuns, & Taffoni 2002). Others have obtained statistical measures of the non-linear density and velocity fields based on ellipsoidal collapse (Fosalba & Gaztanaga 1998a,b; Scherrer & Gaztaaga 2001; Ohta, Kayo, & Taruya 2003, 2004; Lam & Sheth 2008a,b). Angrick & Bartelmann (2010) used this model with additional components introduced to treat the virialization epoch. Very recently, Despali, Tormen, & Sheth (2013) have advocated the use of ellipsoidal halo finders as an improvement over the spherical overdensity method to model shapes of haloes and this method has been applied to big numerical simulations to get insights into the shape distribution of dark matter haloes (Bonamigo et al. 2014). Thus, spherical and ellipsoidal collapse models are not only used in isolation to get insights into the results of simulations, but they are also used in conjunction with numerical techniques to get semi-analytic estimates or for post-processing numerical data.

One of the reasons why these simple geometries are so popular is that exact analytic solutions are available for homogenous perturbations evolving in pure matter cosmologies. The collapse in these cases is self-similar and the axes' lengths (or radius, in case of sphere) are the primary variables of interest. However, the main observationally relevant variables are the density and line of sight velocity, or more generally, the gravitational field and the peculiar velocity field. Thus it is more natural and interesting to directly understand how the these fields evolve in simple geometries. In case of spherical symmetry, the collapse is radial and only two variables suffice to describe the dynamics: density δ and the velocity divergence Θ. In a recent paper Nadkarni-Ghosh (2013), hereafter N13, investigated the dynamics of these variables in a two-dimensional density-velocity divergence phase space [3]. A relation between the two variables was obtained by imposing the criterion of 'no perturbations at the big bang time', and it was shown that this traces out a special curve in the 2D phase-space. The flow of perturbations is such that all perturbations, no matter where they start in phase space, eventually get attracted to this curve. Those that start along the curve, stay on it to a high degree of accuracy. The attracting nature established that this curve [4] was the desired non-linear density-velocity relation and it was found that a combination of analytic forms given by Bilicki & Chodorowski (2008) and Bernardeau (1992) gave a good fit.

In case of a triaxial ellipsoid, the situation is more involved. The full dynamics depends not only on the internal potential, but also on the external tidal field, which has been treated differently by different authors. The internal gravitational potential has a quadratic dependence on the length of the principle axes of the ellipsoid (Peebles 1980). In this paper, we follow the model of Bond & Myers (1996), hereafter BM96, which assumes that the external tidal field is also along the principle axes of the ellipsoid throughout the evolution. The gravity field can then be described by three variables. These correspond to the eigenvalues of the tensor of second derivatives of the gravitational potential (henceforth called the 'gravity Hessian'). In the absence of rotation, the velocity field also needs three variables. These are the eigenvalues of the tensor of partial derivatives

[3] In N13, the velocity perturbation variable was $\theta = \Theta/3$

[4] In N13, this curve was termed the 'Zeldovich curve' because it is the non-linear extension of the 'no decaying modes' criterion, which is invoked in the linear Zeldovich approximation (Zeldovich 1970); here we call it the SC-DVDR

of the velocity field (also sometimes called the 'velocity deformation tensor' [5] and in this work referred to as the 'velocity derivative tensor'). These six variables completely describe the gravitational dynamics of the ellipsoid. Since the potential of the system is intimately connected to its shape, these variables get connected to the eigenvalues of the deformation or displacement tensor.

In this work, we aim to study the joint evolution of density and velocity through the dynamics of these eigenvalues. Starting from the BM96 set of equations for triaxial collapse, we obtain a set of coupled one-dimensional differential equations for the nine eigenvalues. This new set has no dependence on the elliptic functions that appear in the original equations for the axes lengths and is a well-defined dynamical flow. In §2, we derive these equations and by applying the 'no perturbations at the big bang' condition, we get a relation between the eigenvalues of the gravity Hessian and the velocity derivative tensor. This traces out a subspace of perturbations, which we call the 'Zeldovich subspace' and we find a new universal relation that describes the perturbations in this subspace. As a by-product, this analysis gives us insight into the relation between the density and the trace of the deformation tensor. In §3, we examine the dynamics in the 2D $\delta - \Theta$ space. We investigate the scatter in the $\delta - \Theta$ relation and its relation to the velocity shear, thus providing a new insight based on local dynamics. Finally, as an application, in §4, we numerically compute the marginal one-point probability distribution function (PDF) of the density and velocity divergence and compare them to some existing forms in the literature. We conclude in §5. Throughout this paper the terms 'ellipsoidal' and 'triaxial' are used interchangeably.

2 DYNAMICS OF THE ELLIPSOID

2.1 Notation and equations

Consider a uniform ellipsoidal distribution of cosmological fluid consisting of dark matter and dark energy evolving in a flat, homogenous and isotropic background. Let $\rho_{m,e}$ be the matter density inside the ellipsoid. It differs from the background matter density $\bar{\rho}_m$; the difference is characterized by the fractional density $\delta = \rho_{m,e}/\bar{\rho}_m - 1$. The dark energy is the same inside and outside the ellipsoid and is described by a cosmological constant with density ρ_Λ. Let the origin be at the centre of the ellipsoid. The ellipsoid can be completely characterized by the evolution of its three principal axes. In this paper we follow the equations of BM96, which assume that the direction of the axes remains unchanged throughout the evolution. The physical coordinate of each axis r_i can be written as $r_i = a_i(t)q$ $(i = 1, 2, 3)$, where q is the comoving radius of the corresponding 'Lagrangian sphere' (BM96): this is a sphere concentric with the ellipsoid whose mass equals that of the ellipsoid but whose density is the same as the background. a_i are the 'scale factors' of each axis and a is the background scale factor. Throughout this paper we will use the subscript 'i' to index the axes and '$init$' to denote initial conditions. Mass conservation during evolution implies $a^3q^3\bar{\rho}_m = a_1a_2a_3q^3\rho_{m,e}$ giving

$$\delta = \frac{a^3}{a_1a_2a_3} - 1. \tag{1}$$

The evolution of a_i according to BM96 is [6]

$$\frac{d^2a_i}{dt^2} = -4\pi G\left[\frac{\bar{\rho}_m}{3} - \frac{2}{3}\rho_\Lambda\right]a_i - 4\pi G\left[\bar{\rho}_m\left\{\frac{\delta\alpha_i}{2} + \lambda_{ext,i}\right\}\right]a_i, \tag{2}$$

where

$$\alpha_i = a_1a_2a_3\int_0^\infty \frac{d\tau}{(a_i^2+\tau)\prod_{j=1}^{j=3}(a_j^2+\tau)^{1/2}} \quad \text{with} \quad \left(\sum_{i=1}^{3}\alpha_i = 2\right) \tag{3}$$

$$\lambda_{ext,i} = \frac{5}{4}\left(\alpha_i - \frac{2}{3}\right) \quad \text{non-linear approx.} \tag{4}$$

In eq. (2), the first term in square brackets corresponds to the background potential and the second term to the perturbation potential. The α_is are parameters that describe the internal potential of the ellipsoid and are computed using Carlson's elliptic integrals (Carlson 1987, 1989; Press et al. 2002; see appendix B for relations). $\lambda_{ext,i}(t)$ models the external tidal field. In this paper, we will use the non-linear approximation [7]. Using standard definitions: $\bar{\rho}_m = \Omega_m\rho_c$, $\rho_\Lambda = \Omega_\Lambda\rho_c$ and $H^2 = 8\pi G\rho_c/3$

[5] In the past, these have also been referred to as the 'gravitational shear' and 'velocity shear' tensors respectively. However, we will keep this terminology only for the traceless part of these tensors.

[6] Our notation differs slightly from BM96: $\alpha_i \equiv b_i$ and $\lambda_{ext,i} \equiv \lambda'_{ext,i}$ in BM96. With this, the two terms $\frac{\delta}{3} + \frac{\delta b'_i}{2}$ in BM96 are equal to $\frac{\delta\alpha_i}{2}$ in our notation.

[7] A recent paper by Angrick & Bartelmann (2010) experimented with using a hybrid model to compute halo mass functions. They used the non-linear expression of BM96 at early times and reverted back to the linear expression of BM96 after turn-around. They concluded that the hybrid model and the non-linear model gave approximately the same results. We prefer to use a single function than a piecewise one so we stick to the BM96 form

and converting the time variable to a gives

$$\frac{d^2a_i}{da^2} + \left\{\frac{1}{Ha}\frac{d}{da}(Ha)\right\}\cdot\frac{da_i}{da} = -\frac{3}{2a^2}\left[\Omega_m(a)\left(\frac{1}{3}+\frac{\delta\alpha_i}{2}+\lambda_{ext,i}\right)-\frac{2}{3}\Omega_X(a)\right]a_i. \tag{5}$$

Note that the Ω parameters are functions of a and are related to their values today ($a = a_0$) by

$$\Omega_m(a) = \frac{\Omega_{m,0}H_0^2a_0^3}{H^2a^3};\quad \Omega_\Lambda(a) = \frac{\Omega_{\Lambda,0}H_0^2}{H^2}. \tag{6}$$

In this paper we will consider only two cosmologies. The EdS case with $\Omega_m = 1$ and $\Omega_\Lambda = 0$ and the ΛCDM case with $\Omega_m = 0.29$ and $\Omega_\Lambda = 0.71$. The evolution of the ellipse is completely determined once six parameters are known: the three axes lengths $a_{i,init}$ and their velocities $\dot{a}_{i,init}$ at some initial epoch $a_{\rm init}$.

An alternate description of the ellipse can be given by a set of nine *dimensionless* parameters

$$\lambda_{a,i} = 1 - \frac{a_i}{a} \tag{7a}$$

$$\lambda_{v,i} = \frac{1}{H}\frac{\dot{a}_i}{a_i} - 1 \tag{7b}$$

$$\lambda_{d,i} = \frac{\delta\alpha_i}{2} + \lambda_{ext,i}, \tag{7c}$$

where $i = 1, 2, 3$. The eigenvalues $\lambda_{d,i}$ are ordered as $\lambda_{d,1} \geqslant \lambda_{d,2} \geqslant \lambda_{d,3}$. This implies the ordering $\lambda_{v,1} \leqslant \lambda_{v,2} \leqslant \lambda_{v,3}$ and $\lambda_{a,1} \geqslant \lambda_{a,2} \geqslant \lambda_{a,3}$ at all times.

The three λ_a characterize the shape of the ellipse in terms of the deviation from the background. They correspond to the eigenvalues of the 'comoving strain or deformation tensor' (see Appendix A for definitions) . Because the ellipsoid is always deformed along its principle axes, the deformation tensor is diagonal at all times. When an axis is collapsing $\lambda_a \to 1$, whereas for an expanding axes, $\lambda_a \to -\infty$.

The three λ_v capture the deviation of the velocity of each axes from the background Hubble flow. They correspond to the eigenvalues of the tensor of (scaled) velocity derivatives. The trace part gives the 'expansion'

$$\Theta = \frac{\nabla\cdot\mathbf{v}}{H} = \lambda_{v,1} + \lambda_{v,2} + \lambda_{v,3}. \tag{8}$$

where $\mathbf{v} = \dot{\mathbf{r}} - H\mathbf{r}$. In our definition, a negative λ_v implies a infall and a positive λ_v implies expansion. The three eigenvalues completely describe the curl-free velocity field of this model.

The three λ_d correspond to the eigenvalues of the gravity Hessian (tensor of second derivatives of the gravitational field). Equation (7c) comprises of two terms; the first corresponds to the internal potential of the ellipse and the second to the external tidal field or the traceless gravitational tidal tensor. This definition and the fact that $\sum_i \alpha_i = 2$, implies

$$\delta = \lambda_{d,1} + \lambda_{d,2} + \lambda_{d,3}. \tag{9}$$

This is also the consistency condition arising from Poisson's equation.

Not all λs are independent. Equation (7c) defines an implicit relation between the three λ_d and the three λ_a (this can be seen from the definitions of α_i and $\lambda_{a,i}$). In general, this relation is not linear. However, when the perturbations are small, the Zeldovich approximation implies $\lambda_{a,i} = \lambda_{d,i}$ and $\lambda_{v,i} = -\lambda_{d,i}$. Equation (9) reduces to

$$\delta_{\rm lin} = \lambda_{a,1} + \lambda_{a,2} + \lambda_{a,3}. \tag{10}$$

We emphasize that eq. (10) is not valid in the non-linear regime and we will illustrate the difference in §2.3. Usually it is standard to characterize the shape of the ellipse in terms of the 'ellipticity' e and 'prolaticity' p parameters (Bardeen et al. 1986). These are sometimes defined in terms of λ_d, but as has been emphasized in the literature (for e.g., Angrick & Bartelmann 2010), such definitions are valid only in the linear regime. Connecting the shape to $\lambda_{d,i}$ in the non-linear regime necessarily involves solving for the three axes lengths.

An important assumption in the framework of Bond & Myers is that the principle axes of the deformation tensor and gravitational shear tensor coincide at all times during the evolution. If this assumption is violated then the ellipsoid can rotate and additional parameters need to be introduced to describe the dynamics. A more general framework that allows for rotation has been introduced by Eisenstein & Loeb (1995).

In terms of the λ parameters, the equations eq. (5) and its initial conditions are

$$\frac{d^2\boldsymbol{a}}{da^2} + \left\{\frac{1}{Ha}\frac{d}{da}(Ha)\right\}\cdot\frac{d\boldsymbol{a}}{da} = -\frac{3}{2a^2}\left[\Omega_m(a)\left\{\frac{1}{3}+\boldsymbol{\lambda}_d(a)\right\}-\frac{2}{3}\Omega_X(a)\right]\boldsymbol{a} \tag{11}$$

$$\boldsymbol{a}_{\rm init} = a_{\rm init}(1-\boldsymbol{\lambda}_{a,\rm init}) \tag{12}$$

$$\left.\frac{d\boldsymbol{a}}{da}\right|_{a_{\rm init}} = a_{\rm init}(1-\boldsymbol{\lambda}_{a,\rm init})(1+\boldsymbol{\lambda}_{v,\rm init}). \tag{13}$$

We have introduced boldface symbols for quantities that are 3-tuples. The product $(1-\boldsymbol{\lambda}_{a,\rm init})(1-\boldsymbol{\lambda}_{v,\rm init})$ *does not* denote a dot product. It is just the product of the corresponding components for each axes. The boldface $\mathbf{a}$ denotes the axes of the ellipse and a denotes the scale factor of the background.

2.2 Dynamics in phase space

2.2.1 Equations for the eigenvalues

The nine (dimensionless) eigenvalues completely characterize the density, velocity and shape perturbations in this model of ellipsoidal collapse. In this paper, our focus is on the joint dynamics of density and velocity, hence, in principle, only six evolution equations are needed: one for each component of $\boldsymbol{\lambda}_d$ and $\boldsymbol{\lambda}_v$. These are obtained by their definitions in eqs. (7a), (7b) and the evolution given by eq. (11). However, it turns out that the equation for $\lambda_{d,i}$ involves complicated functions of a_i which cannot be inverted easily since in the non-linear regime the relation between λ_d and the axes is implicit (see Appendix B). The system simplifies greatly if one adds the parameters λ_a to the set. Thus, the net system for the nine eigenvalues is

$$\frac{d\lambda_{a,i}}{d\ln a} = -\lambda_{v,i}(1-\lambda_{a,i}) \tag{14a}$$

$$\frac{d\lambda_{v,i}}{d\ln a} = -\frac{1}{2}\left[3\Omega_m(a)\lambda_{d,i} - \{\Omega_m(a) - 2\Omega_\Lambda(a) - 2\}\,\lambda_{v,i} + 2\lambda_{v,i}^2\right] \tag{14b}$$

$$\begin{aligned}\frac{d\lambda_{d,i}}{d\ln a} = &-(1+\delta)\left(\delta+\frac{5}{2}\right)^{-1}\left(\lambda_{d,i}+\frac{5}{6}\right)\sum_{j=1}^{3}\lambda_{v,j} \\ &+\left(\lambda_{d,i}+\frac{5}{6}\right)\sum_{i=1}^{3}(1+\lambda_{v,i}) - \left(\delta+\frac{5}{2}\right)(1+\lambda_{v,i}) \\ &+\sum_{j\neq i}\frac{\{\lambda_{d,j}-\lambda_{d,i}\}\cdot\left\{(1-\lambda_{a,i})^2(1+\lambda_{v,i}) - (1-\lambda_{a,j})^2(1+\lambda_{v,j})\right\}}{(1-\lambda_{a,i})^2-(1-\lambda_{a,j})^2},\end{aligned} \tag{14c}$$

where

$$\delta = \sum_{i=1}^{3}\lambda_{d,i}.$$

In general, the choice of $\lambda_{d,\rm init}$ (or alternatively $\lambda_{a,\rm init}$) and $\lambda_{v,\rm init}$ is independent. However, when the fluctuations are small, one generally employs the Zeldovich approximation (Zeldovich 1970), which states that the velocity is proportional to acceleration and the proportionality constant is set by requiring 'no growing modes' (Buchert 1992; Susperregi & Buchert 1997). Physically, this means that there are no perturbations at the big bang epoch. At early epochs, when $\Omega_m \approx 1$, this gives the relation $\boldsymbol{\lambda}_a = \boldsymbol{\lambda}_d$ and $\boldsymbol{\lambda}_v = -\boldsymbol{\lambda}_d$. More generally, $\boldsymbol{\lambda}_v = -f(\Omega_m)\boldsymbol{\lambda}_d$, where $f(\Omega_m) = \Omega_m^{0.55}$ is the linear growth rate (Linder 2005; we have ignored the weak Λ dependence). The linear density-velocity divergence is

$$\Theta_{\rm lin} = -f(\Omega_m)\delta_{\rm lin}. \tag{15}$$

2.2.2 The Zeldovich subspace

There are two approaches when we consider extension to the non-linear regime. One way is to initialize the system in the linear regime, evolve eqs. (14a) to (14c) into the non-linear regime and analyze the resulting $\boldsymbol{\lambda}_d - \boldsymbol{\lambda}_v$ at any later time. However, there is no guarantee that the resulting 6-tuples are universal; i.e. they may change with initial conditions. An alternate approach is to extend the essence of the Zeldovich approximation into the non-linear regime. That is, given three λ_ds one has to choose the three λ_vs (or vice versa) which satisfy the condition 'no perturbations at the big bang'. This condition sets a special relation between the λ_d and the λ_v and we denote the resulting 6-tuples as $(\boldsymbol{\lambda}_d, \boldsymbol{\lambda}_v^{Zel})$. This set defines a subspace in the 6D phase space which we call the 'Zeldovich subspace'. Since there are only three independent parameters, this space is 3-dimensional. The superscript appears only on $\boldsymbol{\lambda}_v$ to denote $\boldsymbol{\lambda}_v$ is a function of $\boldsymbol{\lambda}_d$ (our convention). Computationally, $\boldsymbol{\lambda}_v^{Zel}$ is obtained as follows. Given the $\boldsymbol{\lambda}_d$, first compute the $\boldsymbol{\lambda}_a$ from the implicit relation eq. (7c). This acts as a known initial condition for eq. (11). Then backward integrate eq. (11) with $\boldsymbol{\lambda}_v$ as a unknown initial value which is solved for three simultaneous conditions $\mathbf{a}(a=0) = 0$. It does not suffice to solve for only one or two of the axes. $\delta = 0$ at $a = 0$ only when all three axes are zero simultaneously. The value for $a_{\rm init}$ is taken to be the epoch for which the $\boldsymbol{\lambda}_d - \boldsymbol{\lambda}_v$ relation is desired.

The two approaches are complementary and it is not obvious that they will give identical results. A different set of initial conditions (for example, those that violated the Zeldovich approximation) could, in principle, generate future $(\boldsymbol{\lambda}_d, \boldsymbol{\lambda}_v)$ values that need not satisfy the non-linear Zeldovich criterion (i.e., no perturbations at the big bang). However, we find that this is not the case. All perturbations, irrespective of whether they initially satisfy the Zeldovich approximation, satisfy the same $\boldsymbol{\lambda}_d - \boldsymbol{\lambda}_v$ relation at late times, suggesting a universal behaviour. This universality is tested as follows. This test is for universality is performed as follows. We track the trajectory of a set of initial points $(\boldsymbol{\lambda}_{d,\rm init}, \boldsymbol{\lambda}_{v,\rm init})$ using the eigenvalue equations and examine how much each trajectory deviates from the Zeldovich subspace at late times. The initial conditions at $a = 0.001$ are drawn from the distribution given below (Doroshkevich (1970); see Rossi 2012 and Angrick 2013 for recent

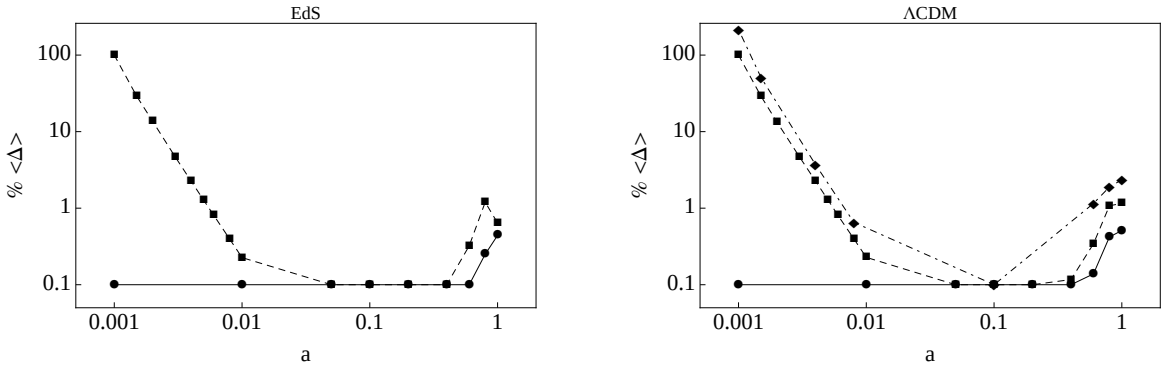

Figure 1. The attracting nature of the Zeldovich subspace: the solid (dashed) lines correspond to $\boldsymbol{\lambda}_{v,\rm init} = -\boldsymbol{\lambda}_{d,\rm init}$ ($\boldsymbol{\lambda}_{v,\rm init} = -2\boldsymbol{\lambda}_{d,\rm init}$). The latter set has a 100% deviation at the initial time $a = 0.001$. For the ΛCDM case an additional non-collinear set $\boldsymbol{\lambda}_{v,\rm init} = (-2,-3,-4)\cdot\boldsymbol{\lambda}_{d,\rm init}$, where $\cdot$ implies component wise product) was considered (denoted by the dot-dashed lines). This set has a initial deviation of 216%. The deviation decreases as a power law in a scaling as $\sim a^{-2.6}$ for both EdS and ΛCDM cosmologies.

extensions)

$$p(\lambda_{d,1},\lambda_{d,2},\lambda_{d,3}) = \frac{15^3}{8\pi\sqrt{5}\sigma_G^6}\exp\left(-\frac{3I_1^2}{\sigma_G^2}+\frac{15I_2}{2\sigma_G^2}\right)\cdot(\lambda_{d,1}-\lambda_{d,2})(\lambda_{d,2}-\lambda_{d,3})(\lambda_{d,1}-\lambda_{d,3}), \tag{16}$$

where $\sigma_G \equiv \sigma_G(R_f)$, the r.m.s. density fluctuation at the scale R_f, $I_1 = \lambda_{d,1}+\lambda_{d,2}+\lambda_{d,3}$ and $I_2 = \lambda_{d,1}\lambda_{d,2}+\lambda_{d,2}\lambda_{d,3}+\lambda_{d,1}\lambda_{d,3}$. This PDF is gives the value at $a = 1$; the value at $a = 0.001$ is obtained by multiplying by the appropriate linear growth factor $D_+(a) = 5\Omega_{m,0}/2\int_0^a[a'H(a')/H_0]^{-3}da$ (Dodelson 2003). Each point is evolved according to eqs. (14a) to (14c). At a future epoch, a point on this trajectory is a 6-tuple denoted by $\{\boldsymbol{\lambda}_d^{evol}, \boldsymbol{\lambda}_v{}^{evol}\}$. For this $\boldsymbol{\lambda}_d^{evol}$, we compute the corresponding $\boldsymbol{\lambda}_v^{Zel}$ as described above. This gives the corresponding point in the Zeldovich subspace denoted as $\{\boldsymbol{\lambda}_d^{evol}, \boldsymbol{\lambda}_v^{Zel}\}$. The distance between $\{\boldsymbol{\lambda}_d^{evol}, \boldsymbol{\lambda}_v{}^{evol}\}$ and $\{\boldsymbol{\lambda}_d^{evol}, \boldsymbol{\lambda}_v^{Zel}\}$ is a measure of how close the trajectory gets to the Zeldovich subspace. We define the relative deviation at any epoch as

$$\Delta(a) = \frac{||\boldsymbol{\lambda}_v^{evol}(a) - \boldsymbol{\lambda}_v^{Zel}(a)||}{||\boldsymbol{\lambda}_v^{Zel}(a)||}, \tag{17}$$

where, $||\mathbf{x}-\mathbf{y}||$ denotes the norm $\sqrt{\sum_i (x_i-y_i)^2}$, $i = 1,2,3$.

Figure 1 shows the average (over 50 points) relative deviation as a function of a for the EdS (left panel) and ΛCDM models (right). For the EdS case, two sets of initial conditions were considered. The first set (solid line) was initialized at $a = 0.001$ using the linear relation: $\boldsymbol{\lambda}_{v,\rm init} = -\boldsymbol{\lambda}_{d,\rm init}$ and the second (dashed line) with $\boldsymbol{\lambda}_{v,\rm init} = -2\boldsymbol{\lambda}_{d,\rm init}$. In the first set, the error between the linear limit and the exact values that lie in the Zeldovich subspace was found to be 0.1%. This value was set as a measure of the tolerance i.e. at any other epoch, the error was chosen to be the maximum of the mean deviation and the tolerance. It was found that at most future epochs, the error stays within 0.1% but rises to about 1% near $a = 1$. The second set of initial conditions corresponds to 100% deviation at $a = 0.001$. The relative deviation drops down exponentially from $\sim 100\%$ at $a = 0.001$ to the sub percent level at $a = 0.1$. This implies that even trajectories that start far off from the Zeldovich subspace eventually find their way onto it. For this set of initial conditions too, the error rises slightly near $a \sim 1$. Similar behaviour is observed for the ΛCDM case. In this case, an additional third non-collinear set (dot-dashed line) of initial conditions was considered $\boldsymbol{\lambda}_{v,\rm init} = \{-2,-3,-4\}\cdot\boldsymbol{\lambda}_{d,\rm init}$ i.e., the x, y and z components are twice, thrice and four times the linear value. The initial deviation in this case is 216%, but again it drops down exponentially. The latter two sets of initial conditions clearly illustrate the attracting nature of the Zeldovich subspace, but the reason for this late time rise is not yet fully clear.

Some insight may be gained by looking at it from the point of view of Lagrangian Perturbation Theory (LPT). The Zeldovich approximation is the first order term in the LPT series (Buchert 1992) and it implies that there are no decaying modes at this order. In this construction, there may be decaying modes in the higher order solution. Requiring that there be 'no perturbations at the big bang' is equivalent to demanding that there be 'no growing modes' at every order in the LPT series (see Ehlers & Buchert 1997; Nadkarni-Ghosh & Chernoff 2013 for the general LPT series construction). Thus, the two solutions, one obtained by imposing 'no growing modes' initially and then evolving and the other obtained by imposing 'no growing modes at every order' are different and the differences could potentially grow at late times. Whether this explains the observed behaviour quantitatively is yet to be understood and is beyond the scope of this paper. Here, it suffices to note that compared to the initial deviation from the Zeldovich subspace (~ 100 %) the final deviation is two orders of magnitude smaller.

In recent work (N13), this technique was applied to spherical perturbations. It was shown that the non-linear density-

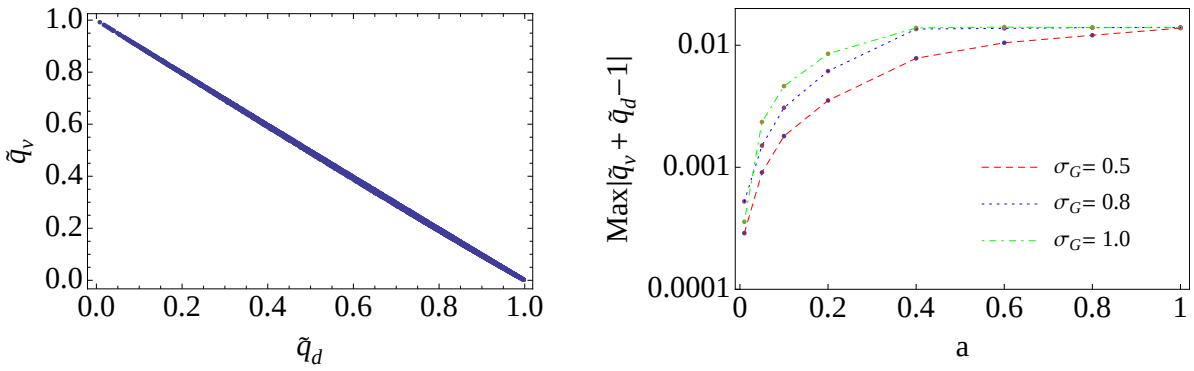

Figure 2. A universal velocity-gravity relation: The left panel plots the triaxiality parameter paris $(\tilde{q}_d, \tilde{q}_v)$ for a single realization ($\sigma_G = 1$ at $a = 1$) in the ΛCDM cosmology. The pairs lie on a straight line defined by $\tilde{q}_v + \tilde{q}_d = 1$. The error in the relation is plotted in the right panel. The error increases with epoch, but stays within 2% for the range of σ_Gs considered here.

velocity relation traced out a universal curve which satisfied the form

$$\Theta_{\rm sph} = \begin{cases} \frac{3}{2}\Omega_m^{\gamma_1}\left[1 - (1+\delta_{\rm sph})^{\frac{2}{3}\Omega_m^{\gamma_2}}\right] & -1 \leqslant \delta_{\rm sph} < 1 \\ \\ \Omega_m^{\gamma_1+\gamma_2}\left[(1+\delta_{\rm sph})^{\frac{1}{6}} - (1+\delta_{\rm sph})^{\frac{1}{2}}\right] & \delta_{\rm sph} \geqslant 1 \end{cases} \tag{18}$$

with $\gamma_1 = 0.56$ and $\gamma_2 = -0.01$ for a ΛCDM cosmology. This density-velocity divergence formula based on spherical collapse is a combination of the forms of Bernardeau (1992) and Bilicki & Chodorowski (2008) and henceforth will be referred to as the 'SC-DVDR'. This curve is time-invariant for an EdS cosmology, but changes for the ΛCDM case due to the variation of Ω_m throughout evolution.

2.2.3 A universal non-linear $\boldsymbol{\lambda}_d - \boldsymbol{\lambda}_v$ relation

We find that it is possible to characterize the universality of the $\boldsymbol{\lambda}_d - \boldsymbol{\lambda}_v$ relation in terms of triaxiality parameters (s and q). These are generally defined in the study of axis ratios (Schneider, Frenk, & Cole 2012; Nadkarni-Ghosh & Singhal 2015), in terms of the major and minor axes or alternatively in terms of the eigenvalues of the deformation tensor. Here, we generalize the definitions to eigenvalues of any 3-dimensional tensor.

$$s = \frac{1-\lambda_{\rm max}}{1-\lambda_{\rm min}} \tag{19}$$

$$q = \frac{1-\lambda_{\rm inter}}{1-\lambda_{\rm min}} \tag{20}$$

$$\tilde{q} = \frac{q-s}{1-s} = \frac{\lambda_{\rm max}-\lambda_{\rm inter}}{\lambda_{\rm max}-\lambda_{\rm min}}, \tag{21}$$

where, $\lambda_{max/min/inter}$ denote the maximum, minimum and intermediate eigenvalues. By construction, $\tilde{q}$ is smaller than unity. We find that, to a very good approximation, the $\boldsymbol{\lambda}_d - \boldsymbol{\lambda}_v$ relation is given by

$$\tilde{q}_v + \tilde{q}_d = 1, \tag{22}$$

where the subscripts d and v refer to the gravity Hessian and the velocity derivative tensor respectively. It is easy to see that this relation is satisfied in the linear regime because $\lambda_{d,max} = -\lambda_{v,min}$ and vice versa. Figure 2 illustrates this relation (left panel) and its accuracy (right panel). The left panel plots the $\{\tilde{q}_d, \tilde{q}_v\}$ pairs for a single realization ($\sim$ 10,000 points) corresponding to $\sigma_G = 1$ at $a = 1$ for the ΛCDM cosmology. As a measure of the accuracy of the relation, we compute $Max|\tilde{q}_v + \tilde{q}_d - 1|$, where the maximum is taken over 50,000 points (five realizations). The right panel plots this error as a function of a for three different values of σ_G. The accuracy of the relation decreases with epoch, but stays within 2%. This relation is a ratio of differences, and since the primary dependence of the velocity-gravity relation is through the linear growth factor, we expect this to be valid for other cosmologies as well (i.e. for other values of Ω_m and Ω_Λ). Thus, it is universal, not only with respect to redshift and the mass scale (σ_G), but also with respect to certain standard dark energy models.

We found the above relation somewhat serendipitously while studying the behaviour of axis ratios Nadkarni-Ghosh & Singhal (2015). The PDF of the $\tilde{q}$ parameter for the deformation tensor turns out to be an invariant of the dynamics (to percent level accuracy), and it was natural to investigate the behaviour of the corresponding $\tilde{q}$ parameter for the gravity Hessian and the velocity derivative tensor. The pattern of the PDFs for $\tilde{q}_v$ and $\tilde{q}_d$ suggested that $\tilde{q}_d + \tilde{q}_v$ was a constant, equal to one. The Zeldovich subspace is three dimensional. To completely describe this subspace analytically, one requires two

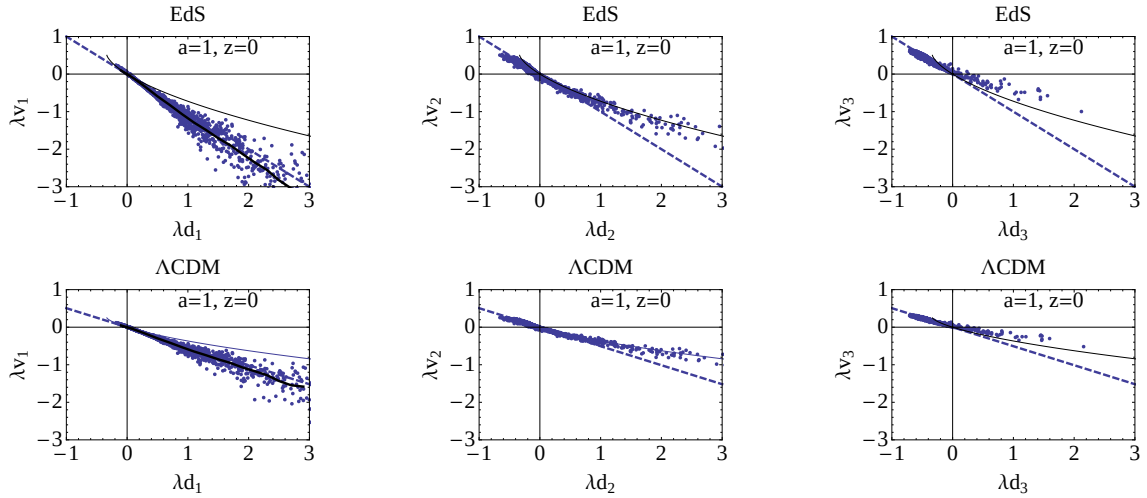

Figure 3. Snapshot at $a = 1$ of the 2D $\lambda_d - \lambda_v$ slices of the subspace. The solid line is the SC-DVDR given by eq. (18) and the dashed line is the linear relation $\lambda_v = -\lambda_d$. The first panel corresponds to the largest eigenvalues. The 'mean' relation between them is very close to the linear relation. This is also responsible for the mean $\delta - \Theta$ relation being close to linear, although to a lesser extent (see figure 5).

additional independent equations connecting the λ_ds and λ_vs. More detailed investigations of the phase space equations will be necessary to construct appropriate invariants and are beyond the scope of this paper.

2.2.4 2D $\lambda_d - \lambda_v$ subspaces

The entire Zeldovich subspace of the 6D phase space cannot be visualized directly. Nevertheless, it helps to visualize 2D subspaces defined by the parameters $(\lambda_{d,i}, \lambda_{v,i})$. Figure 3 shows three such projections at $a = 1$. In each plot, the dotted line shows the linear relation $\lambda_{v,i} = -f(\Omega_m)\lambda_{d,i}$. The solid curved line is the SC-DVDR given by eq. (18); in this case, $\lambda_d = \frac{\delta_{\rm sph}}{3}$ and $\lambda_v = \frac{\Theta_{\rm sph}}{3}$, where $\delta_{\rm sph}$ and $\Theta_{\rm sph}$ are given by eq. (18). The main interesting point observed here is that the 'mean' relation between the largest eigenvalue $\lambda_{d,1}$ and the corresponding $\lambda_{v,1}$ is close to the linear one. It is clear that in the non-linear regime, each axes has a different relation between λ_d and λ_v i.e., the 'vectors' $\boldsymbol{\lambda}_d$ and $\boldsymbol{\lambda}_v$ are no longer proportional. This means that although in the triaxial model, the gravitational shear tensor and velocity derivative tensor always have the same principle axes, their eigenvalues are not simple multiples of each other. This is related to the fact that the gravitational acceleration and peculiar velocity are not parallel to each other in the non-linear regime, which has been discussed earlier in the context of Lagrangian perturbation theory (for e.g., Bagla & Padmanabhan 1996; Susperregi & Buchert 1997; Nadkarni-Ghosh & Chernoff 2013). We also note the distinction between the breakdown of parallelism and breakdown of proportionality; for e.g. for the sphere with a radially dependent overdensity, the acceleration and velocity in the non-linear regime are always parallel at any point (both are radial), but yet as fields they are not proportional.

2.3 δ vs. trace of the deformation tensor

Using the phase space evolution one can also investigate the relation between the exact non-linear density $\delta = \sum_i \lambda_{d,i}$ and its linear approximation $\delta_l = \sum_i \lambda_{a,i}$. Figure 4 shows the difference at three epochs: $a = 0.01, 0.4$ and 1. The dashed line denotes the linear relation and the solid line denotes the relation when all the axes are equal. In this case, $\lambda_a = \delta_{l,\rm sph}/3$, where $\delta_{l,\rm sph}$ is the linear spherical overdensity and from eqs. (1) and (7a) we have

$$\delta_{\rm sph} = \frac{1}{(1 - \frac{\delta_{l,\rm sph}}{3})^3} - 1. \tag{23}$$

The dots indicate the numerically evolved data points. It is clear that at early times the linear approximation is valid, but at later epochs (middle and right panels), it fails for values as low as $\delta_l \sim 0.01$, which are small enough to be considered linear. For example, for some points with $\delta_l = 0.01$, the middle panel ($a = 0.4$) shows the non-linear δ to be 10 times higher. The right panel ($a = 1$) shows it to be 100 times higher. Thus, the linear approximation severely underestimates the actual value of δ and in particular ceases to be valid at late times even for linear densities.

This discrepancy can be understood if one examines the mathematical expressions relating δ and δ_l. From eqs. (1) and

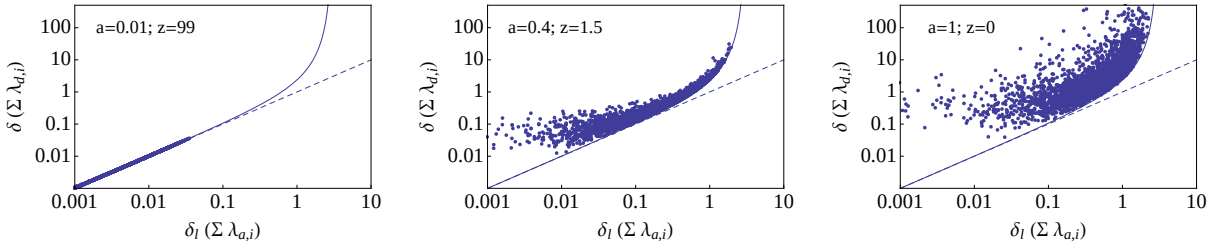

Figure 4. Difference between the exact δ given by $\sum_i \lambda_{d,i}$ and the sum of the eigenvalues of the strain tensor which is used as an approximation.

(7a)

$$\delta = \prod_{i=1}^{3}(1-\lambda_{a,i})^{-1} \tag{24}$$

$$\approx \delta_l + \sum_{i=1}^{3}\lambda_{a,i}^2 + \lambda_{a,1}\lambda_{a,2} + \lambda_{a,2}\lambda_{a,3} + \lambda_{a,1}\lambda_{a,3} + \mathcal{O}(\lambda^3) \tag{25}$$

At early times, all λ_as are small and the second order correction is small for all values of λ_a. However, due to the asymmetry, it is possible to have two values of λ_a large ($\sim \mathcal{O}(1)$) but with opposite signs. This asymmetry is already present in the initial conditions. The initial PDF given by eq. (16) has only 16% probability of generating all λs with the same sign (all positive or all negative). In 84% of the cases, there are atleast two with different signs (this distribution stays more or less constant through the evolution; see Appendix C). Suppose $\lambda_{a,1} = -\lambda_{a,3} \sim \mathcal{O}(1)$ and $\lambda_{a,2}$ is small. Then the second order term reduces to $\lambda_{a,1}^2 \sim \mathcal{O}(1)$, i.e. not small compared to the first order terms. To illustrate this, we consider one sample point in the right panel. This has values $\{\delta_l, \delta\} = \{0.004, 1.134\}$ and the individual $\boldsymbol{\lambda}_a = \{0.708, -0.819, 0.115\}$. The second order terms in this case add up to 0.5, much larger than the linear value. Therefore, strictly speaking, the approximation that $\delta \sim \sum_{i=1}^{3}\lambda_{a,i}$ is valid only at very early epochs $a \lesssim 0.01$.

In passing, we also note that all the data points lie above the solid curve which represents the spherical relation. This can be proven mathematically: for a fixed sum $\sum_i \lambda_{a,i}$, the l.h.s. of eq. (24) is minimum when all the axes are equal.

3 DYNAMICS IN THE $\delta - \Theta$ PLANE.

In this section, we analyse the dynamics in the 2D space corresponding to the variables $\delta = \sum \lambda_{d,i}$ and $\Theta = \sum \lambda_{v,i}$.

3.1 Ellipsoid vs. sphere

The dynamical equations for the variables δ and Θ are given by

$$\frac{d\delta_{\rm ell}}{d\ln a} = -(1+\delta_{\rm ell})\Theta_{\rm ell} \tag{26a}$$

$$\frac{d\Theta_{\rm ell}}{d\ln a} = -\frac{1}{2}\left[3\Omega_m(a)\delta_{\rm ell} - \{\Omega_m(a) - 2\Omega_\Lambda(a) - 2\}\,\Theta_{\rm ell} + \frac{2}{3}\Theta_{\rm ell}^2 + 2\sigma^2\right], \tag{26b}$$

where

$$\sigma^2 = \sum_i \sigma_i^2; \quad \sigma_i = \lambda_{v,i} - \Theta_{\rm ell}/3.$$

σ_is are the eigenvalues of the traceless 'shear' component of the tensor of velocity derivatives. The δ equation follows from the definitions in eqs. (1), (7b) and (8). The Θ equation follows from summing eq. (14b) over all i and using the relation $\sum_i \lambda_{v,i}^2 = \sigma^2 + \Theta_{\rm ell}^2/3$. The corresponding equations for the sphere are (N13)

$$\frac{d\delta_{\rm sph}}{d\ln a} = -(1+\delta_{\rm sph})\Theta_{\rm sph} \tag{27a}$$

$$\frac{d\Theta_{\rm sph}}{d\ln a} = -\frac{1}{2}\left[3\Omega_m(a)\delta_{\rm sph} - \{\Omega_m(a) - 2\Omega_\Lambda(a) - 2\}\,\Theta_{\rm sph} + \frac{2}{3}\Theta_{\rm sph}^2\right]. \tag{27b}$$

Figure 5 shows $\{\delta, \Theta\}$ pairs from one realization of the case $\sigma_G = 1$. The dashed line is the prediction of linear theory given in eq. (15). The solid black line is the SC-DVDR (eq. 18) and it acts as limiting case for the dynamics. We can prove this mathematically by the following arguments. Suppose that at some instant of time the perturbation pairs of the ellipsoid and sphere are the same i.e., $\{\delta_{\rm ell}, \Theta_{\rm ell}\} = \{\delta_{\rm sph}, \Theta_{\rm sph}\}$ and hence both lie on the Zeldovich curve of the sphere. The ellipsoidal pair

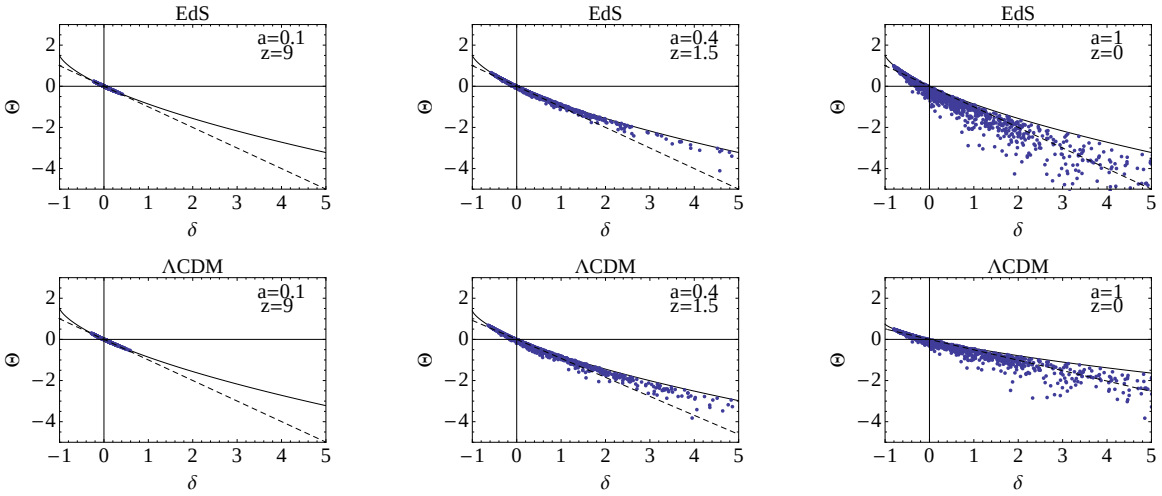

Figure 5. The non-linear $\delta - \Theta$ relation based on triaxial dynamics. The dashed line is the linear relation and the solid line is the SC-DVDR given by eq. (18). At early epochs, both the sphere and ellipsoid obey linear dynamics. Velocity shear effects induce a scatter for the triaxial dynamics. The average $\delta - \Theta$ relation is close to linear, though to a less extent than the $\lambda_{d,1} - \lambda_{v,1}$ relation (see figure 3) because of the contribution from the second and third axes.

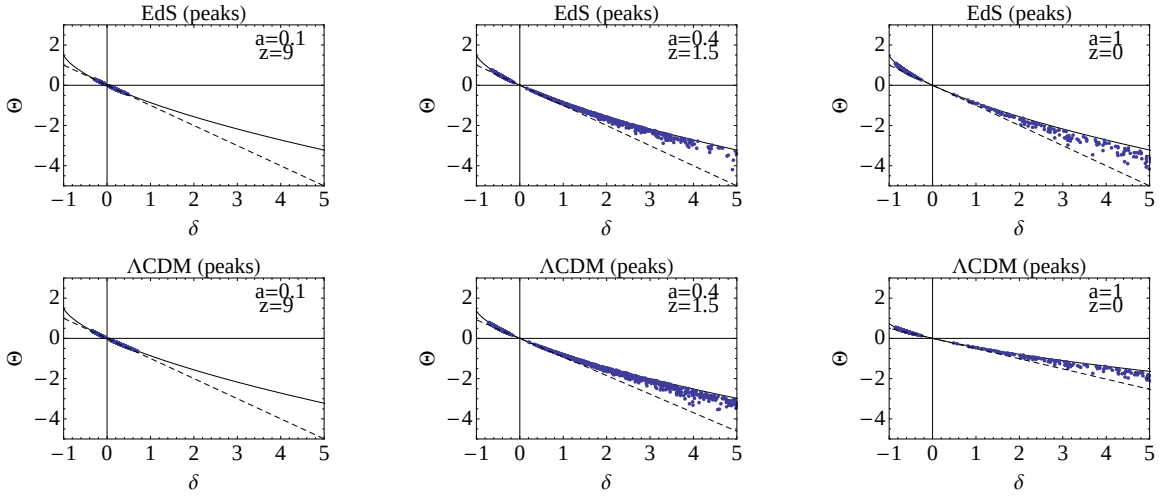

Figure 6. The $\delta - \Theta$ relation for initial conditions such that all λs have the same sign. The values lie much closer to the SC-DVDR than in the general case (figure 5).

is governed by eq. (26) where as the spherical pair is governed by eq. (27). The rate of evolution differs in the two systems; the difference is

$$\left.\frac{d\Theta}{d\delta}\right|_{\rm ell} - \left.\frac{d\Theta}{d\delta}\right|_{\rm sph} = \frac{\sigma^2}{(1+\delta)\Theta}. \tag{28}$$

The terms $(1+\delta)$ and σ^2 are both positive. Thus, when $\Theta < 0$, i.e., the region is contracting, $\left.\frac{d\Theta}{d\delta}\right|_{\rm ell} < \left.\frac{d\Theta}{d\delta}\right|_{\rm sph}$ and when Θ is positive $\left.\frac{d\Theta}{d\delta}\right|_{\rm ell} > \left.\frac{d\Theta}{d\delta}\right|_{\rm sph}$. Since the slope of the SC-DVDR i.e., $\frac{d\Theta}{d\delta}_{\rm sph}$ is always negative, these inequalities imply that triaxiality causes overdense regions to infall faster and underdense regions to expand slower. Triaxiality also implies some regions which are underdense but infalling, a possibility excluded in the spherical model.

It is interesting to note that the linear relation is a good approximation for the mean behaviour at late times. This can be partly explained by comparing with figure 3. The mean relation for the largest (in magnitude) eigenvalues is also close to linear. In this limit the collapse can be modelled as a 1D infall along the largest eigendirection, for which the density-velocity relation is linear (Appendix D).

Numerical simulations solve for the dynamics almost exactly, accounting for a variety of other effects such as non-local physics due to interaction between the environment, accretion etc. However, it is found that the spherical collapse prediction fits the 'mean' $\delta - \Theta$ relation reasonably well (Bernardeau et al. 1999; Kudlicki et al. 2000; Bilicki & Chodorowski 2008). On the other hand, predictions from the ellipsoidal collapse model systematically differ from this relation because of the

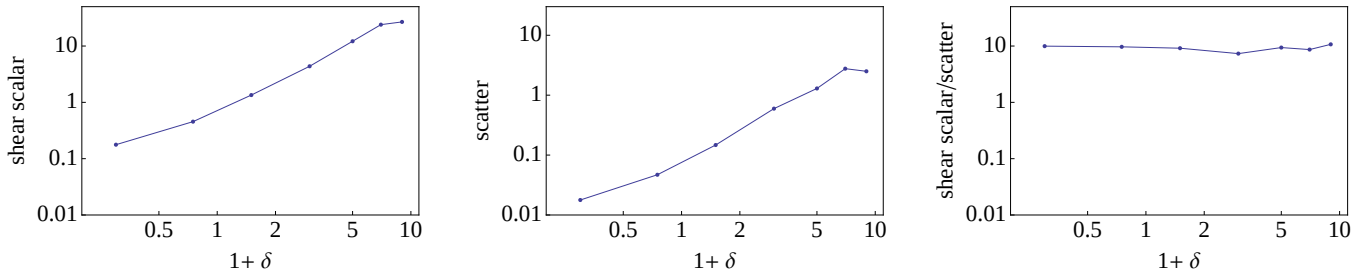

Figure 7. Shear and scatter: the left, middle and right panels show the conditional shear scalar, scatter and their ratio as a function of the density. The conditional shear scalar defined as $\langle\sigma^2\rangle_{|\delta}$ and the conditional scatter as $\left\langle\left(\Theta - \langle\Theta\rangle_{|\delta}\right)^2\right\rangle_{|\delta}$. Both are minimal in the void limit and increase as the density increases. Their ratio is roughly constant indicating that the scatter is related to the non-zero shear, which arises due to the asymmetry in the system.

shear term (see eq. 26). This seemingly better agreement of the spherical collapse model can be roughly explained as follows. The general evolution of the velocity divergence, given by Raychaudhuri's equation, depends on the shear σ^2 and vorticity ($\frac{1}{2}\boldsymbol{\omega}\cdot\boldsymbol{\omega}$). These two terms arise with opposite signs (see Peebles 1980, eq. 22.14); for overdensities, shear speeds up evolution of Θ towards negative values and vorticity does the opposite, possibly causing a partial cancellation at late times. The non-rotating ellipsoidal model includes shear but not vorticity, whereas the spherical collapse includes neither, mimicking the partial cancellation. This argument, while plausible, requires further investigations, but these are beyond the scope of the current paper. The predictions of ellipsoidal collapse agree better if one considers only the peaks (since haloes in simulations form at peaks in the density field). For the case of homogenous triaxial collapse, this corresponds to initial conditions where all the three λ_ds are positive (an infalling halo) or all three are negative (an ever expanding void). Figure 6 shows the phase space snapshot for such special initial conditions evolved using eqs. (14). Clearly, the scatter decreases and the points lie closer to the spherical or 'mean' relation.

3.2 Scatter in the $\delta - \Theta$ plane

The spread in the $\delta - \Theta$ relation is least at the void limit $\delta = -1$ and increases as $\delta \to \infty$. This means that the void limit of the ellipse is the same as the sphere and we can compute it analytically. From eq. (18) this is

$$\Theta_{\rm max} = \Theta|_{\delta=-1} = \frac{3}{2}\Omega_m^{0.56}. \tag{29}$$

We note that the exponent of Ω_m is slightly different from the value of 0.6 given in previous works (Bernardeau et al. 1997; Bernardeau 1992). This is important for proposals to constrain the value of Ω_m using the value of maximal expansion in voids (for e.g. Dekel & Rees 1994).

The non-linear density-velocity divergence relation (DVDR), also known as the gravity-velocity relation, has been discussed in great detail by various authors in the past (Bernardeau 1992; Nusser et al. 1991; Gramann 1993; Bernardeau & van de Weygaert 1996; Chodorowski & Łokas 1997; Chodorowski et al. 1998; Bernardeau et al. 1999; Kudlicki et al. 2000; Ciecielag et al. 2003; Kitaura et al. 2012). These analyses are based on higher order perturbation theory (see review (Bernardeau et al. 2002)), either in Eulerian or Lagrangian frame, or on numerical simulations. All of them show a scatter around the mean-relation which is usually attributed to two reasons. One reason is the non-locality of the dynamics captured by higher order perturbation theory. In linear theory, both in Eulerian space (continuity equation) or in Lagrangian space (Zeldovich approximation), the DVDR relation is local i.e., the velocity divergence/velocity at a point is given by the density/gravitational acceleration at that point. Higher orders of perturbation theory depend on derivatives of lower orders and to determine them, the field needs to be known everywhere (non-local). This non-locality makes the relation stochastic or non-deterministic because although the field equations are deterministic, the initial conditions are random. Another related reason is the traceless 'shear' component of the tensor of velocity derivatives. The eigenvalues of this tensor are $\sigma_i = \lambda_{v,i} - \Theta/3$ and their relation to the scatter has been discussed by Chodorowski (1997) from the point of view of perturbation theory. The triaxial model provides a nice illustration of the same effect based on local dynamics. This is clear from considering eq. (28). The terms that differ from the sphere are all second order and vanish when all the axes are equal. Figure 7 illustrates this effect for the data plotted in figure 5. The left panel plots the (conditional) shear scalar, $\langle\sigma^2\rangle_{|\delta}$, where σ^2 is defined in eq. (27). The shear is small in the void regions and increases in the overdense regions. The middle panel shows the conditional scatter defined as $\left\langle\left(\Theta - \langle\Theta\rangle_{|\delta}\right)^2\right\rangle_{|\delta}$. This has the same trend as that of the conditional shear. The last panel shows their ratio. Interestingly,

this ratio is roughly constant over two decades in density [8]. Thus, the scatter can be attributed to the asymmetry in the system. Indeed, the non-linear DVDR based on the spherical collapse model, which is both local and symmetric, and shows no scatter.

4 MARGINAL PROBABILITIES $p(\Theta)$ AND $p(\delta)$.

As an application of this method, we compute the marginal probabilities $p(\Theta)$ and $p(\delta)$ and qualitatively discuss the joint PDF $p(\delta, \Theta)$.

4.1 Numerical runs

The numerical runs were performed by evolving a set of 10^4 initial conditions using the equations of phase space dynamics given in eq. (14). At the desired final time the δ and Θ are computed according to definitions given in eqs. (9) and (8). Each set was drawn from the distribution given by eq. (16). Three scales were considered: $\sigma_G = 0.5, 1$ and 2. The initial σ_G is related to the scale of the perturbation: the exact dependence depends on the shape and amplitude of the power-spectrum. For the BBKS power spectrum with $n_s = 1$ and $\sigma_8 = 0.9$, $\sigma_G = 0.5, 1, 2$ corresponds to length scales of $R_f = 16.4$,7 and 3.65 h^{-1}Mpc respectively. Two cosmologies were considered: EdS ($\Omega_m = 1, \Omega_\Lambda = 0$) and ΛCDM ($\Omega_m = 0.29, \Omega_\Lambda = 0.71$). The realization at $a = 1$ was the same for the two cosmologies, but the values at the initial epoch $a = 0.001$ were set by multiplying by the correct growth rate factor. By $a = 1$ roughly one-tenth of the points had undergone collapse. For each σ_G value, five realizations were evolved; the PDF is the average over five and the error bars correspond to the standard deviation.

4.2 Theoretical Estimates for comparison

The one-point distributions of the non-linear density and velocity fields have been discussed in great detail in the past. One of the most popular forms for the density PDF is the empirically motivated log-normal model given by Coles & Jones (1991). While this form has been checked by simulations (for e.g., Kayo, Taruya, & Suto 2001, Kitaura et al. 2012), there are others based on more analytical approaches. For example, Kofman et al. (1994) constructed the non-linear PDF from the linear Gaussian PDF by expressing the non-linear density as a function of the linear λ_d via the Zeldovich approximation. Further work by Bernardeau & collaborators (Bernardeau 1994; Kofman et al. 1994) gave forms for the large scale density PDF, both in Eulerian and Lagrangian spaces, from cumulants calculated using perturbation theory. Later Fosalba & Gaztanaga (1998a) gave an alternative approach to computing the cumulants using the spherical collapse model as a local approximation for the dynamics. Ohta, Kayo, & Taruya (2003, 2004) formulated the differential equations for the evolution of the one-point PDFs and solved them using the spherical and ellipsoidal collapse as local approximations for the dynamics. More recently, Lam & Sheth (2008a,b) derived the density PDF both in real space and redshift space based on excursion sets and ellipsoidal collapse.

For the density comparison we choose a combination of the log-normal forms and the perturbative form proposed by Bernardeau (1994):

$$p(\delta) = \begin{cases} p_{B94}^{void}(\delta) & -1 \leqslant \delta < -0.4 \\ p_{L-N}(\delta) & -0.4 \leqslant \delta < 1 \\ p_{B94}^{high}(\delta) & \delta \geqslant 1, \end{cases} \tag{30}$$

where

$$p_{B94}^{void}(\delta)d\delta = \left(\frac{7 - 5(1+\delta)^{2/3}}{4\pi\sigma_\delta^2}\right)^{1/2} (1+\delta)^{-5/3} \times \exp\left[-\frac{9}{8\sigma_\delta^2}\left(-1 + \frac{1}{(1+\delta)^{2/3}}\right)^2\right] d\delta \tag{31}$$

$$p_{L-N}(\delta)d\delta = \frac{1}{\sqrt{2\pi}(1+\delta)\sigma_{ln}} \times \exp\left[-\frac{\{\log(1+\delta) + \sigma_{ln}^2/2\}^2}{2\sigma_{ln}^2}\right] d\delta \tag{32}$$

$$p_{B94}^{high}(\delta)d\delta = f_c \frac{3a_{s\delta}\sigma_\delta}{4\sqrt{\pi}}(1+\delta)^{-5/2} \times \exp\left[\frac{-|y_{s\delta}|\delta + |\phi_{s\delta}|}{\sigma_\delta^2}\right] d\delta \tag{33}$$

with $\sigma_{ln} = \ln(1+\sigma_\delta^2)$, $a_{s\delta} = 1.84, y_{s\delta} = -0.184, \phi_{s\delta} = -0.03$. We have chosen the $n = -3$ values for the parameters a_s, y_s, ϕ_s from B94 (this corresponds to the case of no smoothing). The correction factor $f_c = [1 + 2(0.8 - \sigma_\delta)\sigma_\delta^{-1.3}(1+\delta)^{-0.5}]$ was introduced by B94 to account for the fact that the PDF calculated by the perturbative form did not perform well at high δ.

[8] The ratio is sensitive to the binning in high density regions, but is of the same order of magnitude.

For the velocity divergence the form for $p(\Theta)$ proposed in B94

$$p(\Theta) = \begin{cases} p_{B94}^{void}(\Theta) & 1.5 \geqslant \Theta \geqslant -0.5 \\ \\ p_{B94}(\Theta) & \Theta < -0.5 \end{cases} \tag{34}$$

where

$$p_{B94}^{void}(\Theta)d\Theta = \frac{1}{3}(3+2\tau)^2\sqrt{\frac{1+2\tau}{3\pi\sigma_\Theta^2(3+2\tau)}} \times \exp\left(-\frac{\tau^2}{2\sigma_\Theta^2}\right)d\Theta; \quad \tau = \Theta\left(1-\frac{3}{2}\Theta\right)^{-1} \tag{35}$$

$$p_{B94}^{high}(\Theta)d\Theta = f_c\frac{3a_{s\Theta}\sigma_\Theta}{4\sqrt{\pi}}\left(\frac{3}{2}-\Theta\right)^{-5/2} \times \exp\left[\frac{|y_{s\Theta}|\Theta+|\phi_{s\Theta}|}{\sigma_\delta^2}\right]d\Theta \tag{36}$$

with $a_{s\Theta} = 1.67, y_{s\Theta} = -0.222, \phi_{s\Theta} = -0.042$. The PDF for the ΛCDM cosmology is given by rescaling $p_{\Lambda CDM}(\Theta) = p_{EdS}(\Theta \to \Theta/f(\Omega_m))$, where the σ_Θ is the variance of the scaled variable. The correction factor $f_c = [1+30(0.8-\sigma_\Theta)\sigma_\Theta^{-1.3}(1.5-\Theta)^{-0.5}]$ was introduced in B94 to account for the fact that the expression eq. (36) underestimates the exact answer. We used it only for the case $\sigma_G = 1, a = 1$. For all other cases, $f_c = 1$.

The σ_δ and σ_Θ in the above expressions are related to σ_G using linear theory $\sigma_\delta^2(a) = \sigma_G^2 D_+^2(a)/D_+^2(a=1)$ and not from data. Ideally, these expressions are valid for small values of σ. So we do not compare the case $\sigma_G = 2$ at $a = 1$.

The PDFs generated by our analysis are in the Lagrangian frame since the evolution of the ellipse conserves mass and the density is related to the change in volume. For a fair comparison to the forms discussed above one must convert from the Lagrangian frame to the Eulerian frame. We follow a procedure along the lines discussed in Bernardeau (1994); however, the correct method involves taking derivatives of the Lagrangian PDFs with respect to the mass scale (i.e., varying σ_G). Since we have used only three values of σ, this computation will be highly inaccurate. Instead, we use the linear limit of the relation which, for the case $n = -3$, reads (see appendix E)

$$p_E(\delta) = \frac{p_L(\delta)}{1+\delta} \tag{37}$$

$$p_E(\Theta) = \frac{p_L(\Theta)}{1+\delta}, \tag{38}$$

where p_E and p_L are the Eulerian and Lagrangian PDFs respectively. This correction is applied for each realization and the average is computed over five realizations. The PDFs in either frame are not a priori normalized [9]. We numerically normalize the Eulerian PDF over the range of values considered.

4.3 Results: $p(\delta)$ and $p(\Theta)$

We construct PDFs from the data generated by the numerical runs described in §4.1. The output is analysed at three different epochs: $a = 0.05, 0.4$ and 1 (corresponding to $z = 19, 1.5$ and 0). Three scales were considered: $\sigma_G = 0.5$ (red),1 (blue dotted), 2 (brown, dashed).

Figure 8 shows the marginal probability distribution $p(\delta)$ at the three epochs. The points denote the data and the lines denotes the analytic distribution. The top and bottom panels are the EdS and ΛCDM cosmologies. At early times, the departure from Gaussianity is small and the log-normal model provides a good fit. At later epochs, the fits are better for smaller σ_G. This departure can be attributed to several reasons. Firstly, triaxial collapse is local, whereas higher order perturbation theory can account for non-local effects. The other reason is be that the perturbative approximation fails at high values of δ and the correction factors given in B94 are expected to work only for $\sigma \lesssim 1$. Thirdly, we are using a linear approximation for the transformation from the Lagrangian to Eulerian frame.

The PDF of Θ, shown in figure 9, exhibits a similar behaviour. The x-axis in this case is $\Theta_{\rm max} - \Theta$, where $\Theta_{\rm max}$ is the maximal value in voids given by eq. (29). The point $\Theta_{\rm max}$ in this variable corresponds to $\Theta = 0$ and is shown on the graph. Points to the left of $\Theta_{\rm max}$ correspond to voids and those to the right correspond to overdensities. We see that the analytic expressions given by eq. (34) fit very well at early times when the perturbations are in the linear regime and the agreement reduces with increasing epoch and σ.

4.4 Joint pdf

Figure 10 shows the evolution of the joint PDF $p(\delta, \Theta)$ for the EdS model (left panel) and the ΛCDM model (right panel) at $a = 1$. The region above the SC-DVDR is overlaid to indicate the sharp cut-off observed in figure 5. Our graphs are in reasonably good agreement with the joint PDF plotted by Ohta, Kayo, & Taruya (2003), which was also based on ellipsoidal

[9] Numerically we found that they were normalized with an error of a few percent

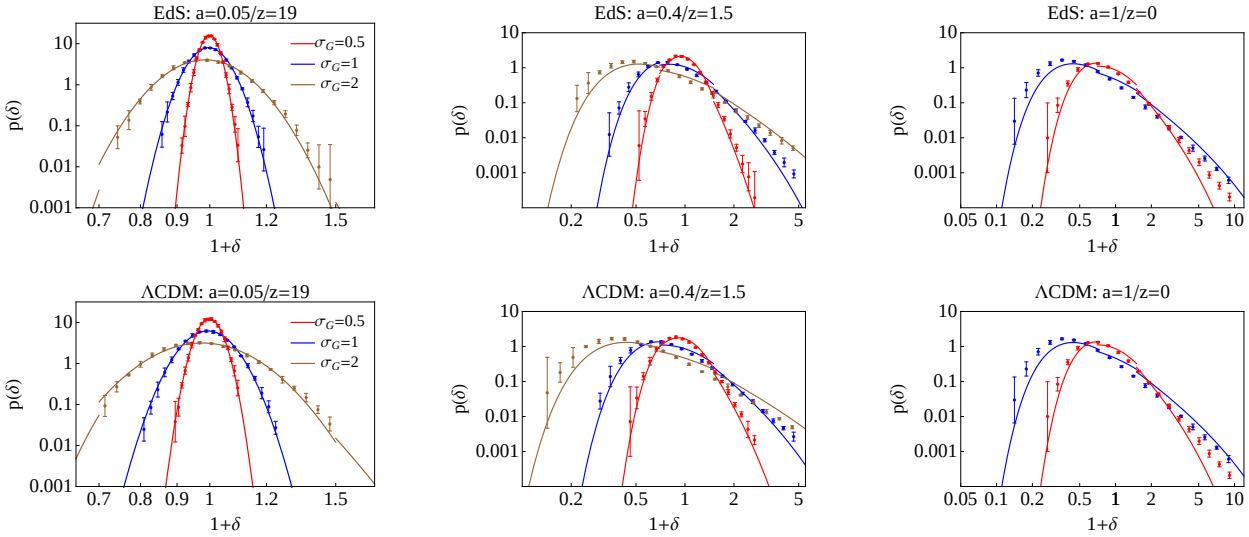

Figure 8. Evolution of $p(\delta)$ vs $1+\delta$ for three values of σ_G for the EdS and ΛCDM models. Agreement with the theoretical forms given in eq. (30) is better in the void regions than in the high density tails.

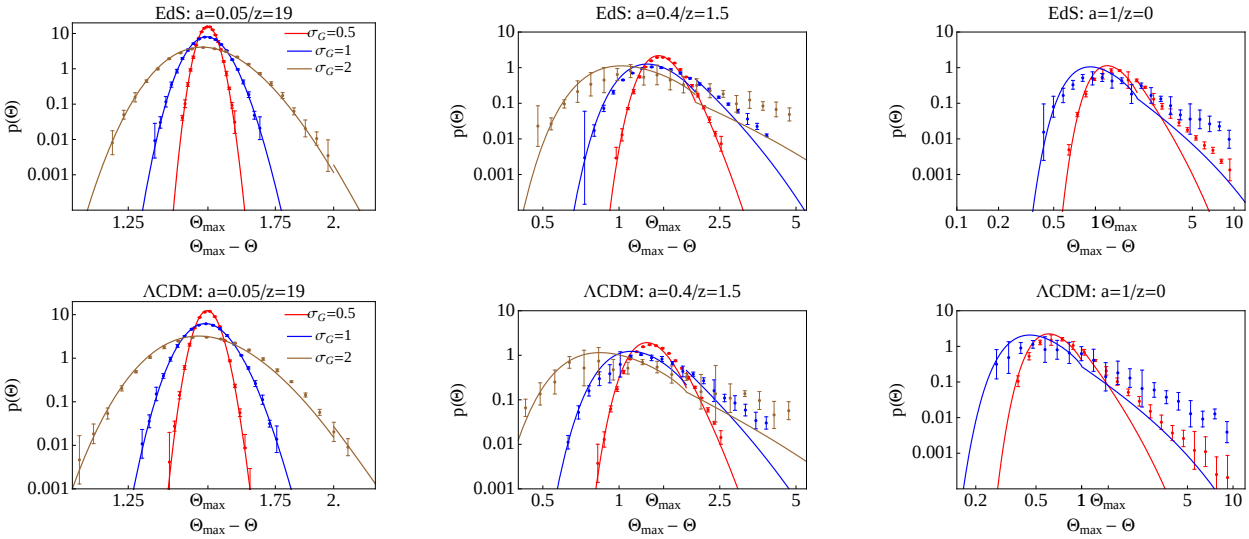

Figure 9. Evolution of $p(\Theta)$ vs $\Theta_{\rm max}-\Theta$, where $\Theta_{\rm max}=1.5\Omega_m^{0.56}$. For EdS, $\Theta_{\rm max}$ is constant with time, where as for ΛCDM it changes. Agreement with the theoretical forms of B94 given in eq. (34) is maintained in voids throughout the evolution, but worsens in the overdense regions $\Theta_{\rm max}-\Theta \gg 1$.

collapse, although they have a slight spill over which may possibly be a plotting artefact. Both for EdS and ΛCDM, the scatter increases as time elapses (at early times the scatter is minimal; all points obey the local linear relation). However, the limiting spherical curve in the two cases is different. The scatter is greater for a higher σ_G (not shown). In N13, it was demonstrated how the attracting nature of the SC-DVDR could be exploited to remove parameter degeneracies related to the power spectrum normalization or index. But the same cannot be done with the joint PDF. Unlike the SC-DVDR which does not depend on the initial σ_G, the joint PDF carries the signature of the initial width (we investigated two more values of σ_G; data not shown).

5 CONCLUSION

The main points of this paper can be summarized as follows.

- We recast the Bond & Myers' set of equations for triaxial collapse into a new set of equations governing the dynamics

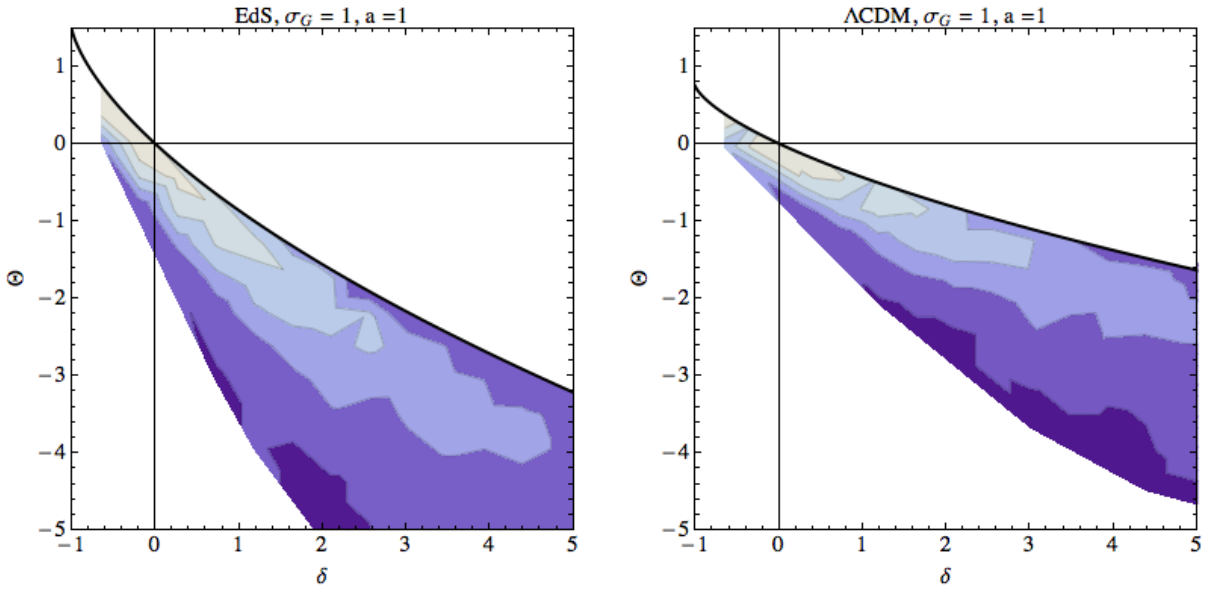

Figure 10. The joint PDF $p(\delta, \Theta)$. The contours are drawn for $p(\delta, \Theta) = 0.32, 0.1, 0.032, 0.01, 0.001$. The SC-DVDR, given by eq. (18), forms a limiting case for the joint PDF. The spread is related to the shear component of the velocity field as was discussed in §3.2

of eigenvalues of the deformation tensor ($\lambda_{a,i}$), the velocity derivative tensor ($\lambda_{v,i}$) and the gravity Hessian ($\lambda_{d,i}$). The main advantage of this reform is that it eliminates the dependence on complicated elliptic integrals which are present in the original system and provides a more natural way to track the dynamics of the perturbation fields. With these definitions $\delta = \sum \lambda_{d,i}$ and the scaled velocity divergence $\Theta = \sum \lambda_{v,i}$, $i = 1, 2, 3$.

• In linear theory 'no decaying modes' implies that the λ_d and λ_v for each axis are proportional, but this breaks down in the non-linear regime. Using the ideas in N13, we extended this to the non-linear regime by imposing the condition 'no perturbations at the big bang'. This gives a relation between the three λ_d and λ_vs at any epoch which traces out a 3D subspace of the 6D perturbation space. We find that along this subspace the perturbations satisfy

$$\tilde{q}_v + \tilde{q}_d = 1, \tag{39}$$

where $\tilde{q} = (\lambda_{\rm max} - \lambda_{\rm inter})/(\lambda_{\rm max} - \lambda_{\rm min})$. To the best of our knowledge, this is a new universal relation, not discussed in earlier literature. Since the dependence on cosmology of the velocity-gravity relation is primarily through the linear growth factor, this universality is with respect to redshift as well as cosmological model.

• Using the same phase space equations, we analysed the relation between the density δ and the trace of the deformation tensor $\sum \lambda_{a,i}$. In the linear regime, $\lambda_{d,i} \approx \lambda_{a,i}$ and $\delta \approx \sum \lambda_{a,i}$. To understand the validity of this statement we examined the $\delta - \sum \lambda_{a,i}$ relation a function of time. We find that linearity of this relation breaks down at late times even for 'linear' δ values. This emphasizes the point that the 'linearity' refers to the individual λs. In the non-linear regime, because of a cancellation between λ_as of opposite signs, it is possible to have a 'linear' δ although the λs are of order unity.

• From the nine-dimensional set for the eigenvalues, we obtained a two dimensional set that governs the $\delta - \Theta$ dynamics. We find that the late time density-velocity divergence relation is close to linear. In this regime, the collapse along the shortest axis dominates the collapse along the other two ones. Therefore, the dynamics can be effectively modelled as a one dimensional with the other two axes comoving with the background.

• When compared to numerical simulations (for e.g., Bernardeau et al. 1999; Kudlicki et al. 2000), triaxial collapse does worse than the spherical collapse in predicting the $\delta - \Theta$ relation. Both triaxial collapse and simulations show a scatter in the relation, but in the first case the spherical relation acts as a upper bound whereas in the case of simulations it turns out to be a good approximation for the mean. In the case of simulations, the scatter arises from random errors coupled with stochastic initial conditions and it is somewhat of a coincidence that the mean relation is well described by the sphere. On the other hand, the scatter in the ellipsoidal model, arises due to the asymmetry in the system and is related to the 'shear' part of the velocity derivative tensor. This effect has been discussed in the past by Chodorowski (1997) using higher order perturbation theory and the triaxial collapse provides a nice illustration of the same based on 'local' dynamics.

• As an application of this method, we examined the pdf of the density and velocity perturbations. We focussed primarily on the marginal PDFs $p(\Theta)$ and $p(\delta)$ and discussed the joint PDF only qualitatively. We find that the agreement is good at earlier epochs and smaller values of σ_G. This is somewhat expected. The theoretical estimates based on perturbation theory

include non-local physics whereas the ellipsoidal model is local. In addition, the conversion from the Lagrangian frame to Eulerian frame is based on a linear relation, which will breakdown for high values of δ. As another application we will consider the evolution of axis ratios (paper II, Nadkarni-Ghosh & Singhal 2015).

The aim of this work was to understand the non-linear behaviour of density and velocity perturbations through the eigenvalue dynamics. This work is general and gives rise to a range of possible applications. In particular, there is recent interest in numerically classifying and quantifying the cosmic web based on eigenvalues of the gravity Hessian (Hahn et al. 2007; Forero-Romero et al. 2009) and the eigenvalues of the velocity derivative tensor (Hoffman et al. 2012; Libeskind, Hoffman, & Gottlöber 2014).One main issue in these studies is that the resultant mathematical structure depends not only on whether one uses the gravitational tensor (T-web) or the velocity tensor (V-web), but it also depends on the details of the classification algorithm (Hoffman et al. 2012; see Forero-Romero et al. 2014 for a list). Furthermore, it was also found that the velocity based classification is a better tracer of the cosmic web and there have been independent observational evidences for the same (Lee, Rey, & Kim 2014). However, the detailed reasoning based on a first principles analysis for this connection is unclear. Through the newly defined 'growth enhancement factor' we are able to characterize the growth rates and provide an insight into this result. Further investigations based on eigenvalue dynamics may help understand these numerical studies better. Another possible application is to improve ellipsoidal collapse based mass function generating codes, such as PINOCCHIO (Monaco et al. 2013). This will be useful to investigate the universal nature of mass function, dependence on cosmology etc. Analytic descriptions of triaxial dynamics can also be used to resolve issues related to alignment or initial shapes of haloes which have been raised in recent simulations (see for e.g. Despali, Tormen, & Sheth 2013) because time-reversing the phase flow equations is easy making it possible to trace back to the initial conditions.

However, there are many limitations of the triaxial model considered here. The first important assumption is that the principle axes stay fixed throughout the evolution i.e., no rotations are included. Second, the ellipse is isolated; the dynamics is local. There are no interactions between neighbours. The effect of the environment is modelled through the effective external non-linear tidal tensor, which depends completely on the axes lengths. The first extension of this analysis would be to follow the more complete set of equations such as those given by Eisenstein & Loeb (1995), which includes rotation. Additional parameters will be required to model the rotational degree of freedom, but the basic framework remains the same. The long-term aim of such investigations would be to provide analytic insight that helps to interpret and improve numerical studies. This paper presents a first step towards this goal.

6 ACKNOWLEDGEMENTS

We would like to thank the referee, Michał Chodorowski, for his detailed comments and suggestions which improved the original manuscript significantly. In addition, we would like to thank Sagar Chakraborty for useful discussions regarding dynamical systems. S.N. would like to thank the hospitality of ICTP, Trieste, and discussions with Pierluigi Monaco and Ravi Sheth which sowed the seeds of this work. Thanks are also due to Pierluigi Monaco for a careful reading of the manuscript and valuable suggestions.

REFERENCES

Angrick C., 2013, ArXiv e-prints, 1305, 497

Angrick C., Bartelmann M., 2010, Astronomy and Astrophysics, 518, 38

Audit E., Teyssier R., Alimi J.-M., 1997, Astronomy and Astrophysics, 325, 439

Bagla J. S., Padmanabhan T., 1996, The Astrophysical Journal, 469, 470

Bardeen J. M., Bond J. R., Kaiser N., Szalay A. S., 1986, The Astrophysical Journal, 304, 15

Bernardeau F., 1992, The Astrophysical Journal, 390, L61

Bernardeau F., 1994, Astronomy and Astrophysics, 291, 697

Bernardeau F., Chodorowski M. J., Łokas E. L., Stompor R., Kudlicki A., 1999, Monthly Notices of the Royal Astronomical Society, 309, 543

Bernardeau F., Colombi S., Gaztaaga E., Scoccimarro R., 2002, Physics Reports, 367, 1

Bernardeau F., van de Weygaert R., 1996, Monthly Notices of the Royal Astronomical Society, 279, 693

Bernardeau F., van de Weygaert R., Hivon E., Bouchet F. R., 1997, Monthly Notices of the Royal Astronomical Society, 290, 566

Bilicki M., Chodorowski M. J., 2008, Monthly Notices of the Royal Astronomical Society, 391, 1796

Bonamigo M., Despali G., Limousin M., Angulo R., Giocoli C., Soucail G., 2014, arXiv:1410.0015 [astro-ph], arXiv: 1410.0015

Bond J. R., Myers S. T., 1996, Astrophysical Journal Supplement Series, 103, 1

Buchert T., 1992, Monthly Notices of the Royal Astronomical Society, 254, 729

Carlson B., 1987, Mathematics of Computation, 49, 595

Carlson B., 1989, Mathematics of Computation, 53, 327

Chodorowski M. J., 1997, Monthly Notices of the Royal Astronomical Society, 292, 695

Chodorowski M. J., Łokas E. L., 1997, Monthly Notices of the Royal Astronomical Society, 287, 591

Chodorowski M. J., Łokas E. L., Pollo A., Nusser A., 1998, Monthly Notices of the Royal Astronomical Society, 300, 1027

Ciecielag P., Chodorowski M. J., Kiraga M., Strauss M. A., Kudlicki A., Bouchet F. R., 2003, Monthly Notices of the Royal Astronomical Society, 339, 641

Coles P., Jones B., 1991, Monthly Notices of the Royal Astronomical Society, 248, 1

Dekel A., Rees M. J., 1994, The Astrophysical Journal Letters, 422, L1

Del Popolo A., Ercan E. N., Xia Z., 2001, The Astronomical Journal, 122, 487

Del Popolo A., Gambera M., 2000, Astronomy and Astrophysics, 357, 809

Despali G., Tormen G., Sheth R. K., 2013, Monthly Notices of the Royal Astronomical Society, 431, 1143

Dodelson S., 2003, Modern Cosmology. Academic Press, Elsevier

Doroshkevich A. G., 1970, Astrophysics, 6, 320

Ehlers J., Buchert T., 1997, General Relativity and Gravitation, 29, 733

Eisenstein D. J., Loeb A., 1995, The Astrophysical Journal, 439, 520

Forero-Romero J. E., Contreras S., Padilla N., 2014, Monthly Notices of the Royal Astronomical Society, 443, 1090

Forero-Romero J. E., Hoffman Y., Gottlber S., Klypin A., Yepes G., 2009, Monthly Notices of the Royal Astronomical Society, 396, 1815

Fosalba P., Gaztanaga E., 1998a, Monthly Notices of the Royal Astronomical Society, 301, 503

Fosalba P., Gaztanaga E., 1998b, Monthly Notices of the Royal Astronomical Society, 301, 535

Gramann M., 1993, The Astrophysical Journal Letters, 405, L47

Hahn O., Porciani C., Carollo C. M., Dekel A., 2007, Monthly Notices of the Royal Astronomical Society, 375, 489

Hoffman Y., Metuki O., Yepes G., Gottlöber S., Forero-Romero J. E., Libeskind N. I., Knebe A., 2012, Monthly Notices of the Royal Astronomical Society, 425, 2049, arXiv: 1201.3367

Icke V., 1973, Astronomy and Astrophysics, 27, 1

Johnson A. et al., 2014, Monthly Notices of the Royal Astronomical Society, 444, 3926

Joyce M., Marcos B., Baertschiger T., 2009, Monthly Notices of the Royal Astronomical Society, 394, 751

Joyce M., Sylos Labini F., 2012, ArXiv e-prints, 1210, 1140

Kayo I., Taruya A., Suto Y., 2001, The Astrophysical Journal, 561, 22

Kerscher M., Buchert T., Futamase T., 2001, The Astrophysical Journal, 558, 79

Kitaura F.-S., Angulo R. E., Hoffman Y., Gottlber S., 2012, Monthly Notices of the Royal Astronomical Society, 425, 2422

Kitaura F.-S., Heß S., 2013, Monthly Notices of the Royal Astronomical Society, 435, L78

Kofman L., Bertschinger E., Gelb J. M., Nusser A., Dekel A., 1994, The Astrophysical Journal, 420, 44

Kudlicki A., Chodorowski M., Plewa T., Ryczka M., 2000, Monthly Notices of the Royal Astronomical Society, 316, 464

Lam T. Y., Sheth R. K., 2008a, Monthly Notices of the Royal Astronomical Society, 389, 1249

Lam T. Y., Sheth R. K., 2008b, Monthly Notices of the Royal Astronomical Society, 386, 407

Lee J., Rey S. C., Kim S., 2014, The Astrophysical Journal, 791, 15

Libeskind N. I., Hoffman Y., Gottlöber S., 2014, Monthly Notices of the Royal Astronomical Society, 441, 1974
Lin C. C., Mestel L., Shu F. H., 1965, The Astrophysical Journal, 142, 1431
Linder E. V., 2005, Physical Review D, 72, 43529
Łokas E. L., 2000, Monthly Notices of the Royal Astronomical Society, 311, 423
Lynden-Bell D., 1964, The Astrophysical Journal, 139, 1195
Majerotto E. et al., 2012, Monthly Notices of the Royal Astronomical Society, 424, 1392
Martino M. C., Stabenau H. F., Sheth R. K., 2009, Physical Review D, 79, 84013
Matarrese S., Pietroni M., 2007, Journal of Cosmology and Astro-Particle Physics, 06, 026
Matsubara T., 2008, Physical Review D, 77, 63530
Monaco P., 1995, The Astrophysical Journal, 447, 23
Monaco P., Sefusatti E., Borgani S., Crocce M., Fosalba P., Sheth R. K., Theuns T., 2013, Monthly Notices of the Royal Astronomical Society, 433, 2389
Monaco P., Theuns T., Taffoni G., 2002, Monthly Notices of the Royal Astronomical Society, 331, 587
Nadkarni-Ghosh S., 2013, Monthly Notices of the Royal Astronomical Society, 428, 1166
Nadkarni-Ghosh S., Chernoff D. F., 2011, Monthly Notices of the Royal Astronomical Society, 410, 1454
Nadkarni-Ghosh S., Chernoff D. F., 2013, Monthly Notices of the Royal Astronomical Society, 431, 799
Nadkarni-Ghosh S., Singhal A., 2015, ArXiv e-prints, 1501, 7075
Nariai H., Fujimoto M., 1972, Progress of Theoretical Physics, 47, 105
Navarro J. F., Frenk C. S., White S. D. M., 1996, The Astrophysical Journal, 462, 563
Nusser A., Dekel A., Bertschinger E., Blumenthal G. R., 1991, The Astrophysical Journal, 379, 6
Ohta Y., Kayo I., Taruya A., 2003, The Astrophysical Journal, 589, 1
Ohta Y., Kayo I., Taruya A., 2004, The Astrophysical Journal, 608, 647
Peebles P., 1980, The Large-Scale Structure of the Universe. Princeton University Press
Press W., Teukolsky S., Vetterling W., Flannery B., 2002, Numerical Recipes in C++. Cambridge University Press
Press W. H., Schechter P., 1974, Astrophysical Journal, 187, 425
Rossi G., 2012, Monthly Notices of the Royal Astronomical Society, 421, 296
Scherrer R. J., Gaztaaga E., 2001, Monthly Notices of the Royal Astronomical Society, 328, 257
Schneider M. D., Frenk C. S., Cole S., 2012, Journal of Cosmology and Astro-Particle Physics, 05, 030
Sheth R. K., Mo H. J., Tormen G., 2001, Monthly Notices of the Royal Astronomical Society, 323, 1
Stabenau H. F., Jain B., 2006, Physical Review D, 74, 84007
Susperregi M., Buchert T., 1997, Astronomy and Astrophysics, 323, 295
White S. D. M., Silk J., 1979, Astrophysical Journal, 231, 1
Wintergerst N., Pettorino V., 2010, Physical Review D, 82, 103516
Zeldovich Y. B., 1970, Astronomy and Astrophysics, 5, 84

APPENDIX A: DEFINITIONS OF THE TENSORS

The physical and comoving axes of the ellipse are

$$r_i = a_i q_i \quad x_i = \frac{a_i}{a} q_i, \tag{A1}$$

where q_i is the initial Lagrangian coordinate of the i-th axis. Initially, the a_i are different from a, so q_i is not the initial comoving coordinate. If we want to characterize the deformation from the sphere then for the sphere $q_1 = q_2 = q_3$. The deformation and velocity are

$$s_i = q_i - x_i = \left(1 - \frac{a_i}{a}\right) q_i \tag{A2}$$

$$v_i = \dot{r}_i - H r_i = \left(\frac{\dot{a}_i}{a_i} - H\right) r_i. \tag{A3}$$

The deformation tensor is

$$e_{ij} = \frac{1}{2}\left(\frac{\partial s_i}{\partial q_j} + \frac{\partial s_j}{\partial q_i}\right) = \lambda_{a,i}\delta_{ij}. \tag{A4}$$

Note that we differ from BM96 by a minus sign. However, their relevant eigenvalues (denoted as $\lambda_{v,A}$) are negative of the eigenvalues of their e_{ij}. We have expressed it so that the λ_a are eigenvalues of e_{ij}. This is just a matter of convention. The important point is that in both conventions $\lambda_a = \lambda_d$ in the linear regime and $\sum \lambda_{a,i} = \delta$. The tensor of velocity derivatives is

$$\frac{1}{2H}\left(\frac{\partial v_i}{\partial r_j} + \frac{\partial v_j}{\partial r_i}\right) = \lambda_{v,i}\delta_{ij}. \tag{A5}$$

The gravitational potential ϕ_p (scaled by $4\pi G\bar{\rho}_m$) for the ellipsoid is

$$\phi_p = \frac{1}{2}\sum_i \lambda_{d,i} r_i^2. \tag{A6}$$

The Hessian of the gravitational potential is

$$\frac{\partial^2 \phi_p}{\partial r_i \partial r_j} = \lambda_{d,i}\delta_{ij}. \tag{A7}$$

The peculiar gravitational acceleration is $\ddot{r} = \nabla\phi_p$. Comparing with eq. (2) one can ensure that the definition is consistent.

APPENDIX B: DERIVATION OF THE PHASE SPACE EQUATIONS

With the definitions of the parameters the equation for the axes evolution takes the form

$$\frac{\ddot{a}_i}{a_i} = -\frac{3H^2}{2}\left(\Omega_m\left\{\frac{1}{3}+\lambda_{d,i}\right\} - \frac{2}{3}\Omega_\Lambda\right). \tag{B1}$$

Ω_m and Ω_Λ are functions of a.

(i) Evolution of $\lambda_{a,i}$: from the definition $\lambda_{a,i} = 1 - \frac{a_i}{a}$, it follows that

$$\dot{\lambda}_{a,i} = -\left(\frac{\dot{a}_i}{a} - \frac{a_i}{a}H\right). \tag{B2}$$

But from the definition of $\lambda_{v,i}$, $\dot{a}_i = Ha_i(1+\lambda_{v,i})$. Substituting in the above equation, using the definition of $\lambda_{a,i}$ and converting from derivatives w.r.t. time to derivatives w.r.t. $\ln a$ gives

$$\frac{d\lambda_{a,i}}{d\ln a} = -\lambda_{v,i}(1-\lambda_{a,i}). \tag{B3}$$

(ii) Evolution of $\lambda_{v,i}$: from the definition $\lambda_{v,i} = \frac{1}{H}\frac{\dot{a}_i}{a_i} - 1$, we have

$$\dot{\lambda}_{v,i} = \frac{\dot{a}_i}{a_i}\left(1 - \frac{1}{H^2}\frac{\ddot{a}}{a}\right) + \frac{1}{H}\left(\frac{\ddot{a}_i}{a_i} - \frac{\dot{a}_i^2}{a_i^2}\right). \tag{B4}$$

Using eq. (B1), the background evolution $\frac{\ddot{a}}{a} = -\frac{H^2}{2}(\Omega_m - 2\Omega_\Lambda)$ and the definitions λ_v gives

$$\frac{d\lambda_{v,i}}{d\ln a} = -\frac{3}{2}\Omega_m\lambda_{d,i} + \lambda_{v,i}\left(-1 + \frac{\Omega_m}{2} - \Omega_\Lambda\right) - \lambda_{v,i}^2. \tag{B5}$$

(iii) Evolution of $\lambda_{d,i}$: $\lambda_{d,i}$ is defined as

$$\lambda_{d,i} = \frac{\delta\alpha_i}{2} + \frac{5}{4}\left(\alpha_i - \frac{2}{3}\right), \tag{B6}$$

where

$$\delta = \frac{a^3}{a_1a_2a_3} - 1, \tag{B7}$$

$$\alpha_i = a_1a_2a_3f_i \tag{B8}$$

$$\text{and} \quad f_i = \int_0^\infty d\tau (a_i^2+\tau)^{-\frac{3}{2}}\prod_{j=1}^{3}(a_j^2+\tau)^{-\frac{1}{2}}. \tag{B9}$$

Hence,

$$\frac{d\lambda_{d,i}}{dt} = \left(\frac{\delta}{2}+\frac{5}{4}\right)\frac{d\alpha_i}{dt} + \frac{\alpha_i}{2}\frac{d\delta}{dt}. \tag{B10}$$

From the definitions,

$$\frac{d\delta}{dt} = -H(1+\delta)\sum_i \lambda_{v,i} \tag{B11}$$

$$\frac{d\alpha_i}{dt} = H\alpha_i\sum_{i=1}^{3}(1+\lambda_{v,i}) + a_1a_2a_3\frac{df_i}{dt}. \tag{B12}$$

The non-trivial part is the term $\frac{df_i}{dt}$. We proceed to evaluate it. Consider the case $i = 1$.

$$\frac{df_1}{dt} = 2a_1\dot{a}_1\int_0^\infty d\tau\left(-\frac{3}{2}(a_1^2+\tau)^{-\frac{5}{2}}(a_2^2+\tau)^{-\frac{1}{2}}(a_3^2+\tau)^{-\frac{1}{2}}\right) - a_2\dot{a}_2I_3 - a_3\dot{a}_3I_2, \tag{B13}$$

where

$$I_3 = \int_0^\infty d\tau(a_1^2+\tau)^{-\frac{3}{2}}(a_2^2+\tau)^{-\frac{3}{2}}(a_3^2+\tau)^{-\frac{1}{2}} \tag{B14}$$

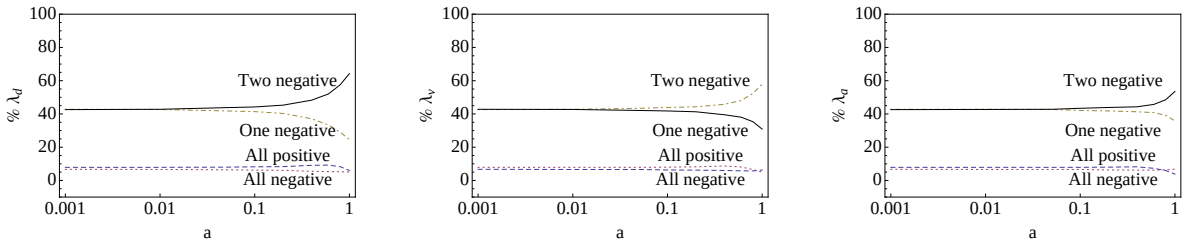

Figure C1. The evolution of the signs of the individual λ parameters. The initial pdf has a distribution of 42% for two eigenvalues λ_d positive or two negative. At early times this is the same for λ_v and λ_a. We find that for all three λ parameters, this distribution evolves in a similar manner changing only slightly at later epochs near $a = 1$.

and I_2 is obtained by interchanging 2 and 3 in I_3. Rewrite $-\frac{3}{2}(a_1^2+\tau)^{-\frac{5}{2}}$ in the first integrand as $\frac{d(a_1^2+\tau)^{-\frac{3}{2}}}{d\tau}$ and integrate by parts to give

$$\frac{df_1}{dt} = -\frac{2}{a_1a_2a_3}\frac{\dot{a}_1}{a_1} + (a_1\dot{a}_1 - a_2\dot{a}_2)I_3 + (a_1\dot{a}_1 - a_2\dot{a}_2)I_2 \tag{B15}$$

The solutions for the integrals I_2 and I_3 can be found in a paper by Carlson (1987); equation 2.10. These expressions give the integrals I_2 and I_3 in terms of $R_F(a_1^2, a_2^2.a_3^2)$.

$$I_3 = \frac{1}{(a_1^2-a_2^2)^2}\left(\frac{2}{3}(2a_3^2 - a_1^2 - a_2^2)R_D(a_1^2,a_2^2,a_3^2) - 4R_F(a_3^2,a_1^2,a_2^2) + \frac{a_1^2+a_2^2}{a_1a_2a_3}\right) \tag{B16}$$

But from relations in Carlson (1989), specifically, equations 2.12, 2.17 and 2.26, it can be shown that

$$3R_F(a_1^2,a_2^2,a_3^2) = a_1^2R_D(a_2^2,a_3^2,a_1^2) + a_2^2R_D(a_3^2,a_1^2,a_2^2) + a_3^2R_D(a_1^2,a_2^2,a_3^2) \tag{B17}$$

where

$$R_D(a_2^2,a_3^2,a_1^2) = \frac{3}{2}\frac{\alpha_1}{a_1a_2a_3}, \quad R_D(a_3^2,a_1^2,a_2^2) = \frac{3}{2}\frac{\alpha_2}{a_1a_2a_3} \quad \text{etc} \tag{B18}$$

Using the two above results from Carlson's paper and the relation $\sum_i \alpha_i = 2$, gives

$$a_1a_2a_3\frac{df_1}{dt} = -2\frac{\dot{a}_1}{a_1} + \frac{(\alpha_2-\alpha_1)(a_1\dot{a}_1 - a_2\dot{a}_2)}{a_1^2-a_2^2} + \frac{(\alpha_3-\alpha_1)(a_1\dot{a}_1 - a_3\dot{a}_3)}{a_1^2-a_3^2} \tag{B19}$$

Using eqs. (B10), (B11), (B12) and (B19) along with the definitions of λ_v and λ_d gives

$$\begin{aligned}\frac{d\lambda_{d,i}}{d\ln a} &= -(1+\delta)\left(\delta+\frac{5}{2}\right)^{-1}\left(\lambda_{d,i}+\frac{5}{6}\right)\sum_{j=1}^{3}\lambda_{v,j} \\ &+ \left(\lambda_{d,i}+\frac{5}{6}\right)\sum_{i=1}^{3}(1+\lambda_{v,i}) - \left(\delta+\frac{5}{2}\right)(1+\lambda_{v,i}) \\ &+ \sum_{j\neq i}\frac{\{\lambda_{d,j}-\lambda_{d,i}\}\cdot\{(1-\lambda_{a,i})^2(1+\lambda_{v,i}) - (1-\lambda_{a,j})^2(1+\lambda_{v,j})\}}{(1-\lambda_{a,i})^2-(1-\lambda_{a,j})^2}.\end{aligned} \tag{B20}$$

Note that only the equation for λ_v depends on the background cosmology. The equations for λ_a and λ_d stay unchanged.

Spherical and linear limits: When all three axes are equal, $\lambda_d = \delta_{\rm sph}/3$ and $\lambda_v = \Theta_{\rm sph}/3$. It is easy to check that the λ_v equation reduces to eq. (27b) for the sphere. For case of the λ_d equation, the last term can be shown to be tending to zero by substituting $\lambda_j = \lambda_i + \epsilon$ and taking the limit $\epsilon \to 0$. The second and third terms cancel and we are left with the first which reduces to eq. (27a). Linearizing the λ_v and λ_d equations gives $d\lambda_{d,i}/d\ln a = -\lambda_{v,i}$ and $d\lambda_{v,i}/d\ln a = \lambda_{v,i}$ giving the correct linear limit $d\lambda_{v,i}/d\lambda_{d,i} = -1$.

APPENDIX C: EVOLUTION OF THE SIGNS OF THE λ PARAMETERS

Figure C1 shows the distribution of the signs of the λ parameters. This distribution stays more or less constant throughout the evolution and may potentially change for initial conditions that are non-Gaussian.

APPENDIX D: PHASE SPACE DYNAMICS FOR 1D COLLAPSE

If the perturbation is only along one axis and the other two axes are comoving with the background, then $\lambda_{d/v,2} = \lambda_{d/v,3} = 0$. Then, $\lambda_{v,1} = \Theta$ and the diagonal components of the shear tensor are $\sigma_1 = \frac{2}{3}\Theta$ and $\sigma_2 = \sigma_3 = -\frac{1}{3}\Theta$. Thus, the dynamical

system given by eq. (26) for an EdS cosmology reduces to

$$\frac{d\delta}{d\ln a} = -(1+\delta)\Theta \tag{D1a}$$

$$\frac{d\Theta}{d\ln a} = -\frac{1}{2}\left[3\delta + \Theta + 2\Theta^2\right], \tag{D1b}$$

Rearrange the terms in the second equation (add and subtract δ and express $\Theta = 3\Theta - 2\Theta$) to give

$$\frac{d\Theta}{d\ln a} = (1+\delta)\Theta - \frac{(\Theta+\delta)(3+2\Theta)}{2}. \tag{D2}$$

Dividing the second equation by the first, gives

$$\frac{d\Theta}{d\delta} = -1 + \frac{(\Theta+\delta)(3+2\Theta)}{2\Theta(1+\delta)} \tag{D3}$$

It is easy to check that a linear relation satisfies this equation. The initial conditions are $\Theta(\delta=0)=0$ and $\frac{d\Theta}{d\delta}\big|_{\delta=0} = c$, where c is some pre-determined constant. Let $\Theta = A\delta + B$ be a solution to the above equation with the given initial conditions. The first initial condition sets $B=0$ and the second one gives

$$\left.\frac{d\Theta}{d\delta}\right|_{\delta=0} = -1 + \frac{3}{2}(A+1) = c, \tag{D4}$$

which in turn sets $A = \frac{2}{3}(1+c) - 1$. For $c=-1$, $A=-1$ giving $\Theta = -\delta$. A similar argument will hold for the ΛCDM case: only the coefficient of Θ changes so the rearrangement of terms will be slightly different and the constant c (or alternatively A) will involve some factors of Ω_m and Ω_Λ.

APPENDIX E: RELATION BETWEEN THE LAGRANGIAN AND EULERIAN PDFS

Given a discrete distribution of massive particles with a mean density $\bar{\rho}$ there are two ways to define the density field. At each point, consider the amount of matter M contained in a *fixed volume* V_0 and define the density contrast as $\delta(M, V_0) = \frac{1}{\bar{\rho}}\frac{M}{V_0}$. This corresponds to the Eulerian prescription. Alternately, in the Lagrangian prescription, at each point one estimates the volume occupied by a *fixed mass* M_0 and the corresponding density contrast is $\delta = \frac{1}{\bar{\rho}}\frac{M_0}{V}$. M_0 and V_0 are related through δ_0 as

$$\delta_0 = \frac{1}{\bar{\rho}}\frac{M_0}{V_0} - 1. \tag{E1}$$

In the Eulerian prescription, δ and M are equivalent variables whereas in the Lagrangian prescription, δ and V are equivalent. Furthermore, a different choice of V_0 for the same choice of M_0 gives a different Eulerian density field and similarly a different choice of M_0 for a fixed choice of V_0 gives a different Lagrangian density field. To relate the PDFs of the Eulerian and Lagrangian fields, note that the probability that a given volume V_0 contains an amount of matter greater than M_0 is same as the probability that M_0 occupies a volume smaller than V_0 (B94 page 702, eq. 33a). This gives

$$\int_{M_0}^{\infty} p_E(V_0, M)dM = \int_0^{V_0} p_L(V, M_0)dV. \tag{E2}$$

To change the integration variable to δ note that

$$p_E(V_0, M) = p_E(V_0, \delta)\left|\frac{d\delta}{dM}\right| \quad \Longrightarrow \quad p_E(V_0, M)dM = p_E(V_0, \delta)d\delta \tag{E3}$$

$$p_L(V, M_0) = p_L(\delta, M_0)\left|\frac{d\delta}{dV}\right| \quad \Longrightarrow \quad p_L(V, M_0)dV = -p_L(\delta, M_0)d\delta. \tag{E4}$$

The negative sign arises in the second equation because δ and V are inversely related. The end points of the first intergal: $M = \{M_0, \infty\} \implies \delta = \{\delta_0, \infty\}$ and in the second $V = \{0, V_0\} \implies \delta = \{\infty, \delta_0\}$. Thus, eq. (E2) becomes

$$\int_{\delta_0}^{\infty} p_E(V_0, \delta)d\delta = \int_{\delta_0}^{\infty} p_L(\delta, M_0)d\delta. \tag{E5}$$

Differentiating w.r.t. δ_0 for a fixed V_0 gives

$$-p_E(V_0, \delta_0) = -\left\{p_L(\delta_0, M_0) + \int_{\infty}^{\delta_0} \frac{\partial}{\partial\delta_0} p_L(\delta, M_0)d\delta\right\}. \tag{E6}$$

The above relation is between the discrete Eulerian and Lagrangian densities. Using the relation between the smooth and discrete densities given by B94 (i.e., the PDFs of the Eulerian densities differ by $1+\delta$, where as the PDFs of the Lagrangian densities are the same) gives

$$(1+\delta_0)p_E(V_0, \delta_0) = \left\{p_L(\delta_0, M_0) - \int_{\delta_0}^{\infty} \frac{\partial}{\partial\delta_0} p_L(\delta, M_0)d\delta.\right\}. \tag{E7}$$

The second term on the r.h.s. depends on the variation of p_L with δ_0 or alternately M_0. Ideally, to compute it we need to know how p_L varies with M_0. A different mass scale corresponds to a different choice of σ. So we can rewrite

$$\frac{\partial p_L}{\partial \delta_0} = \frac{\partial p_L}{dM_0}\frac{\partial M_0}{d\delta_0} \tag{E8}$$

$$= \frac{\partial p_L}{d\sigma}\frac{\partial \sigma}{\partial M_0}\frac{\partial M_0}{\partial \delta_0} \tag{E9}$$

$$= \frac{\partial p_L}{d\sigma}\frac{\partial \sigma}{\partial R_f}\frac{\partial R_f}{\partial \delta_0}, \tag{E10}$$

where in the last equality we have introduced the filtering scale R_f which corresponds to the mass scale M_0 through

$$M_0 = \frac{4}{3}\pi R_f^3 \bar{\rho}. \tag{E11}$$

Combining the above with eq. (E1),

$$(1+\delta_0)V_0 = \frac{4}{3}\pi R_f^3 \tag{E12}$$

and differentiating w.r.t. δ_0 at a fixed V_0 gives

$$\frac{dR_f}{d\delta_0} = \frac{R_f}{3(1+\delta_0)}. \tag{E13}$$

Since $\frac{d\sigma}{dR_f}$ and $\frac{dR_f}{d\delta_0}$ do not depend on δ, eq. (E7) becomes

$$(1+\delta_0)p_E(V_0,\delta_0) = \left\{ p_L(\delta_0,\sigma) - \frac{d\sigma}{dR_f}\frac{dR_f}{d\delta_0}\int_{\delta_0}^{\infty}\frac{dp_L(\delta,\sigma)}{d\sigma}d\delta. \right\}. \tag{E14}$$

In eq. (E14), p_L corresponds to the non-linear probability distribution, however, the numerical studies in this paper were performed with only a few values of σ and the dependence of the distribution on σ cannot be known accurately. Instead, we examine the linear limit to obtain an analytic result and extend the result to the quasi-linear regime. This procedure can be partially justified by arguing that the theoretical results of B94 (the Eulerian pdf that we compare with) are expected to be valid only for small σ.

In the linear regime,

$$p_L(\delta) = \frac{1}{\sqrt{2\pi}\sigma}\exp\left(-\frac{\delta^2}{2\sigma^2}\right). \tag{E15}$$

$$\frac{dp_L}{d\sigma} = -\frac{1}{\sqrt{2\pi}\sigma^2}\exp\left(-\frac{\delta^2}{2\sigma^2}\right) + \frac{\delta^2}{\sqrt{2\pi}\sigma^4}\exp\left(-\frac{\delta^2}{2\sigma^2}\right). \tag{E16}$$

and the integral becomes

$$\int_{\delta_0}^{\infty}\frac{dp_L(\delta,\sigma)}{d\sigma}d\delta = \frac{e^{-\frac{\delta_0^2}{2\sigma^2}}\delta_0}{\sqrt{2\pi}\sigma^2} = \frac{\delta_0}{\sigma}p_L. \tag{E17}$$

It remains to compute $\frac{d\sigma}{dR_f}$ in eq. (E14). This depends on the power spectrum and the window function.

$$\sigma^2(R_f) = \int P(k)W^2(kR_f)d^3k \tag{E18}$$

Assuming a Gaussian filter $W(kR_f) = \exp -\frac{k^2R_f^2}{2}$ and a power spectrum with index n i.e., $P(k) = c_0k^n$, where c_0 is some constant,

$$\sigma^2 = \frac{c_0}{2}R_f^{-(n+3)}\Gamma\left(\frac{n+3}{2}\right); \quad 2\sigma\frac{d\sigma}{dR_f} = -\frac{n+3}{R_f}\sigma^2 \tag{E19}$$

and

$$\frac{d\sigma}{dR_f} = -\frac{(n+3)}{2}\frac{\sigma}{R_f}. \tag{E20}$$

Putting together eqs. (E13), (E14), (E17) and (E20), gives

$$(1+\delta_0)p_E = p_L\left[1 + \frac{(n+3)}{6}\frac{\delta_0}{1+\delta_0}\right]. \tag{E21}$$

In our comparisons, we used $n=-3$. In this case, σ is independent of the smoothing scale and the relation is simply

$$p_E(\delta_0) = \frac{p_L(\delta_0)}{1+\delta_0}. \tag{E22}$$

Arguing that the density-velocity divergence relation is the same in both frames (mean velocity divergence is computed from

the velocity field (within a fixed volume in the Eulerian case and within a fixed mass in the Lagrangian case), the velocity PDFs also have the same relation:

$$p_E(\Theta) = \frac{p_L(\Theta)}{1+\delta}. \tag{E23}$$

The Eulerian PDFs predicted by our analysis and the ones used for comparison are both normalized numerically.